The impact of the North Atlantic Oscillation on climate through its influence on the Atlantic Meridional Overturning Circulation

Thomas L. Delworth[1] and Fanrong Zeng[1]

[1]Geophysical Fluid Dynamics Laboratory/NOAA

201 Forrestal Rd.

Princeton, NJ 08540 USA

Accepted in Journal *of Climate*

November 9, 2015

Corresponding author: Thomas L. Delworth

E-Mail: tom.delworth@noaa.gov
Phone: 609-452-6565

Postal:
Geophysical Fluid Dynamics Laboratory/NOAA
201 Forrestal Rd.
Princeton University Forrestal Campus
Plainsboro, NJ 08540
USA

Abstract

The impact of the North Atlantic Oscillation (NAO) on the Atlantic Meridional Overturning Circulation (AMOC) and large-scale climate is assessed using simulations with three different climate models. Perturbation experiments are conducted in which a pattern of anomalous heat flux corresponding to the NAO is added to the model ocean. Differences between the perturbation experiments and a control illustrate how the model ocean and climate system respond to the NAO. A positive phase of the NAO strengthens the AMOC by extracting heat from the subpolar gyre, thereby increasing deepwater formation, horizontal density gradients, and the AMOC. The flux forcings have the spatial structure of the observed NAO, but the amplitude of the forcing varies in time with distinct periods varying from 2 to 100 years. The response of the AMOC to NAO variations is small at short time scales, but increases up to the dominant time scale of internal AMOC variability (20-30 years for the models used). The amplitude of the AMOC response, and associated oceanic heat transport, is approximately constant as the timescale of the forcing is increased further. In contrast, the response of other properties, such as hemispheric temperature or Arctic sea ice, continues to increase as the time scale of the forcing becomes progressively longer. The larger response is associated with the time integral of the anomalous oceanic heat transport at longer time scales, combined with an increased impact of radiative feedback processes. We show that NAO fluctuations, similar in amplitude to those observed over the last century, can modulate hemispheric temperature by several tenths of a degree.

1. Introduction

One of the central challenges in climate research is to increase our ability to quantify the role of natural variability and anthropogenic forcing in observed climate change (Bindoff et al. 2013). We seek to quantify what fraction of observed changes in the climate system has come from anthropogenic and natural radiative forcing changes, and what fraction from internal variability. A key goal is therefore to improve our understanding of the mechanisms of natural climate variability, particularly on decadal and longer timescales.

Two important phenomena associated with climate variability are the North Atlantic Oscillation (NAO) and the Atlantic Meridional Overturning Circulation (AMOC). These two phenomena have been associated with a wide range of climate variations across the Northern Hemisphere on a variety of time scales (Hurrell 1995, 1996; Hurrell and Deser 2009; Trigo et al. 2002). The NAO is primarily an atmospheric phenomenon, characterized by sub-seasonal to multidecadal variations in storm tracks over the North Atlantic sector (Gerber and Vallis 2009). Extensive previous work has shown that atmospheric circulation changes associated with the NAO drive an array of climate variations over North America and Europe (Scaife et al. 2008; Cullen et al. 2002; Trigo et al. 2002). These variations are clearly linked with changes in large-scale atmospheric circulation and corresponding precipitation and temperature anomalies.

The AMOC consists of a northward flow of relatively warm, salty water in the upper layers of the Atlantic, and a southward return flow at depth (Kuhlbrodt et al. 2007). The associated release of heat to the atmosphere at higher latitudes of the North Atlantic has a major impact on climate and climate variability. A rich history of modeling studies (Delworth et al. 1993; Visbeck et al. 1998; Zhu and

Jungclaus 2008; Park and Latif 2008; Biastoch et al. 2008; Vellinga and Wu 2004; Frankcombe et al. 2010; Danabasoglu et al. 2012a; Medhaug et al. 2012; Menary et al. 2012; Kwon and Frankignoul 2012; Tulloch and Marshall 2012; Yeager and Danabasoglu 2012) has shown that the AMOC can have substantial variability on decadal to centennial time scales. In addition, the AMOC can have a significant influence on climate on many time scales (Delworth and Mann 2000; Knight et al. 2005; Frierson et al. 2013; Frankignoul et al. 2013). Variations in the AMOC are viewed as an important driver of the observed Atlantic Multidecadal Oscillation, which in turn influences hemispheric climate (Zhang et al. 2007; Chylek et al. 2009; Sutton and Dong 2012; Li et al. 2013; Steinman et al. 2015).

Previous modeling work has shown a clear connection between the NAO and the AMOC (Visbeck et al. 1998; Delworth and Greatbatch 2000; Delworth and Dixon 2000; Eden and Jung 2001). Variations in the NAO have been hypothesized to play a role in AMOC variations by modifying air-sea fluxes of heat, water, and momentum. These flux variations alter vertical and horizontal density gradients in the subpolar North Atlantic, thereby inducing changes to deepwater formation and the AMOC.

In this study we examine the connections between NAO variations, the AMOC, and larger scale climate through the use of large suites of climate model simulations. We design experiments to specifically examine how variations in surface fluxes associated with the NAO can induce AMOC variations, and how these AMOC variations in turn influence large-scale climate. We adopt an idealized modeling framework that allows us to examine how different timescales of NAO variations influence the AMOC and the larger climate system. Our methodology involves the use of simulations in which we artificially impose NAO-like fluxes on the model ocean, and assess the response of the model ocean and larger-scale climate to these NAO-like variations. Recent work has suggested that multidecadal

NAO variations can be used as a predictor of Northern Hemispheric temperature (Li et al. 2013), and in this study we conduct simulations that provide a physically based underpinning for that connection.

2. Models and experimental design

a. Models

We use three versions of GFDL climate models in this study. The first is the GFDL CM2.1 model (Delworth et al. 2006). This is a fully coupled ocean-atmosphere model, with land and atmospheric resolution of approximately 200 km in the horizontal, and 24 vertical levels in the atmosphere. The ocean component has horizontal resolution of approximately 100 km, with finer resolution in the tropics, and 50 levels in the vertical. This model has been used in a wide variety of studies of climate variability, predictability and change, and extensive model output from past studies is available at http://nomads.gfdl.noaa.gov/CM2.X/ and http://nomads.gfdl.noaa.gov:8080/DataPortal/cmip5.jsp. The second model used is called CM2.5_FLOR (Vecchi et al. 2014a), referred to here as "FLOR", where "FLOR" stands for Forecast oriented Low Ocean Resolution. This model uses atmospheric physics that are very similar to CM2.1, but has a higher spatial resolution in the atmosphere as well as a much improved land model (LM3) (Milly et al. 2014). The horizontal resolution of the atmosphere and land model is approximately 50 km (versus 200 km in CM2.1). The number of vertical levels in the atmosphere has increased from 24 in CM2.1 to 32 in FLOR. The ocean component of FLOR is similar to that in CM2.1. The third model used is CM3 (Donner et al. 2011; Griffies et al. 2011). This has a similar horizontal spatial resolution in the atmosphere as CM2.1, but has substantially increased vertical resolution (48 layers), as well as including representations of the indirect effect of aerosols and interactive chemistry. As in the other two models, the horizontal resolution of the ocean component is approximately 1°.

Millennial-scale control simulations have been conducted with each model using radiative forcing conditions representative of "preindustrial" conditions, corresponding to approximately calendar year 1860.

b. Experimental design

We wish to assess how the model ocean responds to idealized variations in the NAO, and then alters the rest of the climate system. In particular, we wish to study the response of the AMOC to idealized NAO variations, and how those changes in the AMOC impact the rest of the climate system. We do this by designing simulations in which the model ocean "feels" an arbitrary phase of the NAO. In these simulations we intervene in the model whenever the model atmosphere and ocean exchange fluxes (described in detail below). As a result, the model ocean reacts to arbitrarily imposed NAO flux anomalies. By comparing the differences between ensembles of simulations with and without this artificial NAO forcing, we can assess how the AMOC and model climate system responds to the NAO.

We first create patterns of flux forcing that correspond to the NAO. We start with time series of monthly mean surface fluxes (heat, water, momentum) from the ECMWF-Interim reanalysis (Dee et al. 2011), as well as the time series of the observed NAO using a station-based index (downloaded from the NCAR/UCAR climate data guide at https://climatedataguide.ucar.edu/climate-data/hurrell-north-atlantic-oscillation-nao-index-station-based; the NAO index is defined as the difference between a normalized time series of SLP from Lisbon, Portugal and a normalized time series of SLP from Reykjavik, Iceland, using seasonal means December-March). We then create 4-month averages from the ECMWF-interim reanalysis data over the December-March period. We compute the linear regression coefficients at each grid point between the time series of the reanalysis fluxes (heat, water, and momentum) and the NAO. In Figure 1 we show the regression map for surface heat flux anomalies, indicating the pattern of surface heat flux change accompanying a one standard deviation increase in the NAO. For use as described below, we scale the ECWMF-derived regression coefficients for the flux fields by one standard deviation of the NAO index time series. We use the flux forcing only over the Atlantic from the Equator to 82°N, including the Barents and Nordic Seas. We adjust the fluxes so that their areal integral is zero. In this manner, the imposed heat fluxes do not provide a net heating or cooling to the system.

The coupled models normally compute air-sea fluxes of heat, water and momentum that depend on the gradients in these quantities across the air-sea interface. In our perturbation experiments this process continues, but after these fluxes are calculated we add an additional flux component to the model ocean. The model ocean therefore receives the fluxes that are computed based on air-sea gradients, plus an extra flux that corresponds to a specified phase of the NAO. We have conducted simulations with additions of heat, water, and momentum fluxes. However, sensitivity studies have shown that for this model the heat flux anomalies dominate the response, and so we show results from simulations that are driven only by adding anomalous heat fluxes.

We create time series of NAO-derived fluxes that have idealized variations in time. In one set of experiments, referred to as “switch-on”, we suddenly turn on the extra NAO flux forcing at an arbitrary point in the control simulation, and leave these extra fluxes on with a constant amplitude corresponding to one standard deviation of the observed NAO time series. These experiments elucidate the adjustment process of the climate system in response to an instantaneous imposition of the extra NAO fluxes. We also conduct suites of experiments in which we add NAO fluxes whose amplitude is modulated sinusoidally in time with a single time scale. We conduct separate ensembles of simulations in which the NAO is modulated with periods of 2, 5, 10, 20, 50, and 100 years. The amplitude of the extra NAO forcing time series corresponds to one standard deviation of the observed NAO time series. We note that these are highly idealized sequences of NAO forcing that allow us to systematically examine the response of the ocean to various timescales of NAO forcing, and are not meant to represent the observed NAO time series. In all experiments the NAO forcing is applied only in the months of December through March, with a constant value for that period, and a linear taper at the start and end of this period. This is the primary season of oceanic convection and deepwater formation at higher latitudes of the North Atlantic.

Analyses of the spectral characteristics of the observed NAO suggest that it is fairly similar to white noise, with variance on all time scales, but with some suggestion of spectral peaks around 2 years and 7-10 years(Gámiz-Fortis 2002), as well as multidecadal variability(Li et al. 2013). However, the shortness of the instrumental record means that the robustness of the peaks is questionable, especially at longer time scales (Wunsch 1999). Our simulations are designed to probe the response of the climate system to idealized NAO forcing across a wide range of time scales, consistent with a white noise process that contains variance at all time scales.

In order to more clearly identify the response to the NAO, all experiments are conducted as ensembles. For the CM2.1 simulations we use ten-member ensembles. The ten-members start from 10 different points in a long control simulation, with each of the points separated by 40 years. This separation is longer than the dominant time scale of AMOC internal variability in the model in order to reduce the likelihood of aliasing effects. For analysis we examine the ensemble mean of the perturbed experiments, and contrast that with the ensemble mean of the corresponding sections of the control simulation. For FLOR and CM3 we use five-member ensembles, primarily because of the greater computational expense associated with the higher resolution models.

In our experimental design we can impose NAO-related fluxes of heat, water, or momentum. Preliminary simulations (not shown) have indicated that variations in heat flux have a dominant impact on the AMOC in these models for the decadal-scale variability being examined. Therefore, in subsequent experiments we only impose NAO-related changes in heat flux. However, it is possible that the ocean model used here does not respond as energetically to momentum fluxes as it should, possibly as a consequence of its relatively coarse resolution. Additional studies with higher resolution models that produce more energetic flow should reassess this issue. This is particularly relevant in light of the impact of observed wind stress anomalies for AMOC variability on interannual time scales (Roberts et al. 2013).

We have conducted simulations using NAO-related surface fluxes as defined both from the ECMWF-Interim reanalysis, and as evaluated from a long control integration of the CM2.1 model (pattern shown in Fig. 1b). Since the results were fairly similar when using either set of fluxes to construct the anomaly forcing, we show here only results using the reanalysis forcing. An additional benefit is that such forcings could also be used in similar experiments with other models.

3. Simulated AMOC: mean and variability

We show in Figure 2 the time-mean streamfunction from control simulations of the three models. All show a robust AMOC, with substantial cross-equatorial flow. The AMOC is largest in the CM2.1 model. For each model we compute an index of the AMOC as the maximum value of the annual mean overturning streamfunction between 20°N and 65°N in the North Atlantic. We form time series of the AMOC index for each model. We show the time series and their spectra in the bottom two panels of Figure 2. All the spectra are characterized by significant peaks on interdecadal time scales. The peak in CM2.1 occurs around 15-20 years, around 26-30 years in FLOR, and 30 years in CM3. By performing identical experiments in models with differing AMOC characteristics we hope to gain some measure of the robustness of results. We do not attempt in this study to identify the factors responsible for the differing AMOC characteristics in these models.

4. Response to "switch-on" of NAO forcing

As a first test we use CM2.1 to simulate the response of the AMOC and climate system to suddenly turning on and maintaining an anomalous positive NAO flux forcing whose amplitude corresponds to one standard deviation of the NAO time series. Shown in Figure 3 is the time series of the response of the AMOC at 45°N to the NAO heat flux forcing. This is computed as the ten-member ensemble mean AMOC in the NAO flux forcing run minus the ten-member ensemble emean AMOC from the corresponding control simulation with no externally imposed NAO forcing. The simulated ensemble-mean AMOC adjusts over a decadal scale, increasing in amplitude by several Sverdrups (Sv; 1 Sv = 10^6 $m^3 s^{-1}$). Physically, the NAO related fluxes extract heat from the subpolar gyre and Labrador Seas. This increases near-surface density, mixed layer depths, the rate of deepwater formation, and zonal upper ocean density gradients across the North Atlantic in the latitude range of 45°N to 75°N. These factors tend to enhance the AMOC (Danabasoglu et al. 2012b). Note also that the AMOC response is not steady, but varies, with relative maxima around years 10-13 and 25-28. The time scale of these variations is similar to the time scale of internal variability in CM2.1 (15-20 years as shown in in Figure 2). This similarity of time scales suggests that some of the processes important for the adjustment of the AMOC to this imposed forcing may also be involved in the mechanisms of the dominant timescale of AMOC variability in this model. The response of the model to a switch on of NAO-related fluxes may be a useful way to assess the internal variability timescale of a model, and to delineate some of the important processes that control that timescale. This would be most relevant for models in which the NAO plays a dominant role for ocean decadal-scale variability, and less relevant for models in which other patterns of atmospheric variability, such as the East Atlantic Pattern, are dominant for ocean decadal variability.

We show the spatial structure of this adjustment process in more detail in Figure 4. This contains the climatological mean of several quantities in the top row from a long control simulation. Subsequent rows show the time-evolving response of those quantities to the imposed NAO forcing, calculated as the ensemble mean of the simulations with the NAO forcing minus the ensemble mean of the simulations without the NAO forcing. Each row from the second row to the bottom denotes a later time after the imposition of the NAO fluxes. The sequence of panels show the adjustment of mixed layer depth, AMOC, northward ocean heat transport, SST, and SSS to the additional NAO flux. The imposed anomalous NAO heat flux in the subpolar gyre and Labrador Sea (see Figure 1) leads to near-surface cooling and increased mixed layer depths (see the results in the second row for Lag 3, corresponding to 3 years after the imposition of the NAO fluxes). Convection is enhanced along with a slight strengthening of the AMOC. As we move to larger time lags (successively lower rows in the figure) the enhanced mixed layer depths are maintained, the AMOC continues to strengthen and the region of the enhanced AMOC expands southward. This enhanced AMOC increases ocean heat transport (middle column), leading to positive SST and SSS anomalies throughout the subpolar gyre and portions of the Nordic Seas. This tendency continues throughout the first decade.

5. Sensitivity of impact to timescale of forcing

a. Hemispheric time series

The "switch-on" experiment is useful in illustrating the overall response of the AMOC to NAO fluxes, but we can also probe this relationship by imposing NAO-related fluxes with well-defined timescales, and assessing how the AMOC responds to differing timescales of forcing. Specifically, we create time series of anomalous fluxes that have the spatial pattern of the NAO, but whose amplitude is modulated in time by a sine wave with arbitrary periods. We have conducted 10-member ensembles of such experiments with CM2.1 using periodicities of 2, 5, 10, 20, 50, and 100 years, and evaluated the AMOC and climate system response to these forcings. We show in Figure 5 time series of the AMOC for simulations with various timescales of NAO-related flux forcing. Also shown in each panel (red curve) is the AMOC time series that is calculated as an ensemble average from the ten corresponding segments of the control simulation. The simulations with shorter timescales of forcing are run for shorter durations. The top panel shows simulations with timescales of 2 and 5 years, in addition to the control. The NAO-induced variability of the AMOC is quite small, and is not distinguishable from the mean of the corresponding segments of the control. The middle panel shows results from forcings with periodicities of 10 and 20 years. There is a substantial increase in the response of the AMOC to the forcing, particularly for the 20-year timescale. The bottom panel shows results from forcing at timescales of 50 and 100 years. The AMOC fluctuates at the timescale of the forcing, but the amplitude is similar to that at 20 years.

We can characterize the response at each timescale by the standard deviation of the ensemble mean AMOC time series. Figure 6a shows the standard deviation of the AMOC as a function of the timescale of the forcing. It is clear that the response is small at short timescales of forcing and increases until reaching a timescale close to the characteristic internal time scale of the model AMOC variability (~20 years). The amplitude of the AMOC response does not substantially vary as we further increase the timescale of the forcing. The largest response at a timescale of 20 years may be indicative of a resonant response of the system when forced at the preferred timescale of variability. We show in Fig. 6b the same quantity for ocean heat transport at 23°N summed over all longitudes, and note very similar behavior (the response in the Pacific is small, so we obtain essentially the same result if we compute ocean heat transport only in the Atlantic).

We expect that variations in the AMOC and oceanic heat transport may influence extratropical Northern Hemisphere surface air temperature (NHSAT) and Northern Hemisphere sea ice mean thickness (NHSI). NHSAT is computed by averaging annual mean surface air temperature for all model points poleward of 23°N, and NHSI is calculated by averaging annual mean sea ice thickness poleward of 55°N. We show in Figures 6c and 6d the amplitudes of variations of NHSAT and NHSI. We note that, as was the case with the AMOC and heat transport, variations are small at short time scales and increase up to 20 years. However, in contrast to the AMOC, the amplitude of NHSAT and NHSI variations continues to increase with the timescale of the forcing, such that the amplitude of the response for NHSI at a 100 year forcing timescale is two to three times the amplitude of the response for forcing at 20 years. Why is there a continued increase in the amplitude of the NHSAT and NHSI variations when the amplitudes of the AMOC and oceanic heat transport variations are approximately constant for timescales longer than 20 years? There are multiple contributing factors. First, the time integral of the ocean heat transport anomalies is important for the climate response; this time integral is approximately three times larger for the 100-year forcing than for the 20-year forcing, leading to a larger response. In addition, in response to a warming of the climate system there is reduced snow cover and sea ice, thereby leading to a positive albedo feedback. This amplifies the signal at longer time scales, which is already larger due to the larger time-integral of the heat transport changes. Shown in Figures 6e and 6f are the amplitudes of the variations of the air-sea heat flux and the net upward shortwave radiation at the top of the atmosphere (both quantities are averaged from 23^{o}N to 90^{o}N). The amplitude of the variations of these terms continues to grow for timescales longer than 20 years, indicating these play an increasingly important role at longer timescales.

To more clearly illustrate these relationships we show in Figure 7 the time series of various quantities for two sets of simulations with NAO forcing timescales of 20 years (black curves) and 100 years (red curves). The responses of the AMOC and ocean heat transport have similar amplitudes for the two timescales of forcing, consistent with Figure 6.

The larger response of surface air temperature for the 100-year timescale forcing relative to the 20-year timescale forcing is apparent in Fig. 7c. The amplitude of the response is significantly larger, and the variance of the temperature response is approximately three times larger for the 100-year forcing than for the 20-year forcing. Shown in Fig. 7d are similar curves for Arctic mean sea ice thickness; the variance increases by more than a factor of 3 between the 20-year forcing and the 100-year forcing, despite similar (or even smaller, see Fig. 6a and 6b) amplitudes of AMOC and oceanic heat transport variations at 100 years relative to 20 years. These results suggest that the climatic relevance of NAO-induced AMOC variations increases substantially with timescale. The larger amplitude of the temperature response at longer timescales is at least partially attributable to the greater role of feedbacks in the system. At high latitudes the cryosphere responds to the warming or cooling induced by AMOC variations, and these cryospheric changes in turn influence the amount of shortwave radiation reflected to space, acting as a positive feedback on the system. The time series of anomalies of upward shortwave radiation at the top of the atmosphere are shown in Fig. 7e – the variance increase by a factor of 1.5 from the 20-year forcing to the 100-year forcing. This positive albedo feedback is more effective at longer timescales as progressively more of the cryosphere is altered by the NAO-induced AMOC changes, and therefore participates in the positive feedback. We also show the time series of average air-sea heat flux poleward of 23°N in Fig. 7f. The variance of the air-sea heat flux time series also increases in the 100-year forcing case relative to the 20-year forcing case by a factor of 2. As the amount of sea ice decreases, more open ocean is available to flux heat more effectively from the ocean to the atmosphere; since the sea ice extent is more powerfully impacted on longer timescales, this air-sea heat flux term is also stronger for longer time scales. However, this term is somewhat limited by the total anomalous heat transport in the ocean.

The above suggest that NAO-induced changes in the AMOC create changes in ocean heat transport that drive hemispheric scale variations in surface air temperature and sea ice. In addition, the effect becomes much stronger at long time scales due to the greater time-integral of the ocean heat transport changes and feedback processes associated with changes in snow cover and sea ice.

b. Heat budget diagnostics

We next examine in Figure 8 the changes in oceanic and atmospheric heat transport, as well as changes in the top of the atmosphere radiation balance, generated by the simulations with 100-year NAO flux forcing using CM2.1 (results from the 50-year forcing simulations are similar). In Fig. 8a we plot the linear regression coefficients of the time series of the NAO forcing with itself at various lags; this provides a visual perspective for interpreting the phasing of the changes shown in Figs. 8b and 8c. We show in Figure 8b the linear regression coefficients of poleward oceanic heat transport at 50^{o}N (integrated over all depths) versus the NAO flux forcing time series at various lags (where negative lags refer to times before a maximum of the NAO forcing). We find (not shown) that variations in Pacific transport are extremely small compared to changes in Atlantic heat transport, and so we show only changes in Atlantic heat transport. The ocean heat transport variations are in phase with the NAO flux forcing. We also show that changes in poleward atmospheric heat transport are smaller in amplitude and opposite in sign to the ocean heat transport changes, consistent with the idea of Bjerknes compensation (Bjerknes 1964; Shaffrey and Sutton 2006; Yang et al. 2013). The atmospheric heat transport changes act as a negative feedback on the system. Enhanced (reduced) ocean heat transport warms (cools) the higher latitudes, thereby reducing (increasing) the meridional temperature gradient in the atmosphere and decreasing (increasing) the poleward atmospheric heat transport.

We next decompose the ocean heat transport variations into gyre and overturning components, calculated using monthly data at each model level as:

$$m\ C_p VT = m\, C_p\, (v'T + \overline{V}T\ \ ) \quad (1)$$

where m denotes the mass of water, C_p is the heat capacity of sea water, V denotes meridional velocity in the ocean, T is ocean temperature, the overbar denotes the zonal mean across the Atlantic, and the prime denotes the deviation from that zonal mean. We calculate linear regressions between these heat transport components and the NAO forcing, and show these in Fig 8b. The overturning component (second term on right side of (1), labeled as "moc" on the figure) dominates the total heat transport changes, but there is still a significant role for gyre variations (first term on right side of (1)). The gyre changes appear to lead the overturning changes.

In Fig. 8c we show the regression coefficients of changes in the top of the atmosphere radiation balance versus the NAO forcing (where the radiation terms are calculated as the integral for all points poleward of 50^{o}N). The net radiation at the top of the atmosphere lags the ocean heat transport, and is a negative feedback. Variations in outgoing longwave radiation and net shortwave radiation (netsw) are also shown. It is clear that enhanced (decreased) ocean heat transport warms (cools) the high latitudes which then emit more (less) longwave radiation to space. This dominates the radiation variations. However, the netsw term acts as a positive feedback. Physically, warming (cooling) of the higher latitude regions reduces (increases) the amount of sea ice and snow cover, thereby reducing (increasing) albedo and increasing (decreasing) the amount of shortwave radiation absorbed in the system. This shortwave feedback opposes the damping by longwave radiation, and therefore helps to amplify the warming signal. This is more pronounced at longer time scales of forcing.

The larger response at longer time scales is partially attributable to greater amplification from shortwave radiation forcing. In addition, the time integral of the ocean heat transport is considerably larger for the 100 year NAO forcing than for shorter time scales, since the anomalous ocean heat transport is maintained for a longer period. The time integral of the anomalous poleward oceanic heat transport reaches a maximum of $2.31*10^{22}$ J for the 20-year NAO forcing versus a maximum of $6.62*10^{22}$ J for the 100-year NAO forcing. This substantially larger time integral of heating translates into considerably larger climatic impacts, as shown in Figure 6 and below.

c. Spatial patterns of response

We show in Figures 9-13 the spatial patterns of the responses to the NAO-induced AMOC variations. The responses are computed as the linear regression of the time series of the response for each variable (forced experiment minus control) versus the time series of anomalous NAO flux forcing, and are scaled such that the values shown represent the response to a two standard deviation NAO forcing (meant to illustrate the difference between a one standard deviation positive NAO phase and a one standard deviation negative NAO). We note that, for simplicity, we are using a fixed spatial pattern of the NAO, whereas in reality this pattern changes in time. The responses for the January-March (JFM) season for both timescales of forcing are in Figures 9 and 10, and for July-September (JAS) in Figure 11 and 12. These months are chosen to emphasize responses in winter and summer sea ice as well as changes in precipitation and tropical atmospheric circulation of relevance for tropical cyclone development. We show maps corresponding to the lags of maximum response in extratropical mean surface air temperature.

The Northern Hemisphere (NH) cold season responses for the two timescales are shown in Figures 9 and 10, and show a clear sensitivity to timescale. Surface air temperature changes (Fig. 9a and 9e) show warming at high latitudes, but the warming is larger and more extensive for the 100-year forcing. In particular, the warming signal extends over most of the Eurasian continent in the 100-year forcing case, but is largely confined to oceanic regions of the North Atlantic and Arctic in the 20-year forcing case. The precipitation response is shown in panels b and f. There is a general increase in precipitation over the North Atlantic for both timescales in response to the generally warmer upper ocean. One exception is the notable decrease off the northeast coast of North America in the 20-year forcing case. This is associated with local cooling associated with a southward shift of the recirculation gyre (Zhang and Vallis 2007). This effect is muted at the 100-year timescale where the warming of the North Atlantic is more pervasive. The changes in sea level pressure (SLP) are shown in panels c and g. In both cases there is reduced SLP over the North Atlantic, but the larger scale structure over the Northern Hemisphere differs between the two cases. On the longer time scale there is a tendency for reduced SLP over the entire regions of the North Atlantic and the Arctic, whereas there is a more structured pattern at the shorter time scale. In the upper troposphere (panels d and h) there is a structure response at the shorter time scale of forcing, with regions of increases and decreases, but a more uniform increase in geopotential heights across the Northern Hemisphere at the longer time scale.

The sea ice changes for the JFM season are shown in Figure 10. For the 20-year forcing sea ice changes are confined to the Labrador and Nordic seas, but the changes extend over the entire Arctic for the 100-year forcing case.

We show in Figure 11 results for the July-September (JAS) season. The contrasts in the response of surface air temperature and sea ice thickness between the two timescales of forcing is similar to the winter season. The summer precipitation response is shown in panels b and g. Consistent with previous work the stronger AMOC leads to a northward migration of the Intertropical Convergence

Zone (ITCZ) and associated rainfall, particularly over the African/Atlantic sector (Vellinga and Wu 2004; Zhang and Delworth 2005). This effect is considerably stronger in response to the 100-year forcing. For sea level pressure there is more consistency in the responses between the timescales, with reduced slp over the North Atlantic and Arctic. This reduction in slp over the Atlantic is consistent with analyses of the instrumental record (Sutton and Hodson 2005). Changes in 300 hPa geopotential height are shown in panels d and i – the difference is striking. For the 20-year forcing there is a modest impact, but for the 100-year forcing there is a widespread increase of geopotential heights over the Northern Hemisphere, extending as far south as 40°S. These changes in geopotential height are consistent with the changes in the vertical shear of the zonal wind (hereafter referred to as shear), shown in panels e and j. There is a substantial reduction in shear over the tropical and subtropical North Atlantic in the 100-year forcing case, with a generally smaller overall impact for the 20-year case. This suggests that NAO-induced AMOC changes would substantially influence tropical storm activity for the 100-year forcing case, although the model used for this study does not have sufficient resolution to explicitly simulate tropical storms.

The sea ice response for JAS is shown in Figure 12. While there is very little impact for the 20-year forcing case, there is a pan-Arctic reduction in sea ice thickness for the 100-year forcing case.

We show in Figure 13 the changes in sea surface height induced by the NAO forcing. As shown previously, the AMOC increases in response to positive NAO forcing; this is consistent with an enhanced zonal gradient in sea level height, with negative anomalies along the North American coast and positive anomalies in the mid-Atlantic. These results suggest that decadal scale variations in the NAO induce decadal-scale sea level changes (Goddard et al. 2015; McCarthy et al. 2015) along portions of the eastern coast of North America, with short term trends in sea level change of up to 10 cm per decade. Note that sea level heights along the east coast of North America tend to fall in response to a sustained positive NAO, and rise in response to a sustained negative NAO. This process can therefore contribute substantially to local decadal-scale sea level variations. Additional analyses show that the pattern of sea level height changes propagates to the southwest, more rapidly with the 20-year NAO forcing than the 100-year NAO forcing. The amplitude of the sea level changes is similar for the 20-year and 100-year forcing cases, consistent with similar changes in the AMOC for the two forcing cases. In terms of rates of change in sea level, this implies that the 20-year forcing would have a much greater impact on decadal-scale changes in sea level than the 100-year forcing. Their spatial structures differ somewhat, with more of the changes extending through the Labrador Sea and into Baffin Bay for the 100-year forcing. Both patterns, however, are consistent with modulation of the zonal gradient of sea level consistent with AMOC variations.

6. Sensitivity of impact to model and mean base state

The previous sections examined how the response of the AMOC and larger-scale climate to NAO variations depends on the time scale of the NAO forcing using a single model (CM2.1). In this section we explore how the response to NAO forcing depends on the model's characteristics, including its mean state. We make use of two additional models, FLOR and CM3, as described in section 2a. For all three models we conduct "switch-on" experiments in which heat fluxes corresponding to a positive phase of the NAO are suddenly applied to the model ocean. These simulations are 60 years in duration, with the anomalous flux forcing held constant (but applied only in the months of December-March). Using this simple model design we wish to compare the AMOC and climatic responses among the three models. We conduct 10-member ensembles for CM2.1, and 5-member ensembles for FLOR and CM3 (we use smaller ensembles for FLOR and CM3 due to the greater computational cost of the higher-resolution models).

We show in Figure 14 the AMOC and surface air temperature responses for the three models. All have an increase in AMOC and zonal mean surface air temperature in response to the switch on of the NAO forcing, but there are modest differences in the time scale and amplitude of the response. Part of this may be sampling issues, and part may be due to the differing physical characteristics of each model.

The overall amplitude of the temperature response is largest in FLOR, possibly related to the thicker and more extensive sea ice in the climatological mean state of FLOR (not shown), especially in the Labrador, Nordic and Barents seas. This offers the potential for greater albedo feedback and temperature response. While CM3 has the longest time scale of internal AMOC variability among the three models (see spectral analysis in Figure 2), it appears to respond the most rapidly to the switch on of the NAO forcing. In comparing CM2.1 and FLOR, the AMOC response appears to fluctuate on a longer time scale in FLOR compared to CM2.1, consistent with the longer time scale of internal variability in FLOR (see Figure 2). Despite the above differences, the overall characteristics of the responses are similar, suggesting some degree of robustness in the response.

We also compare the models in their response to a periodic NAO forcing. We select a timescale of 50 years NAO forcing for the comparison. Based on the results of the previous section the response at 20-year forcing was somewhat muted and therefore not a good choice for the comparison. In addition, the computational cost of performing 100-year forcing experiments was substantial for the higher resolution FLOR and CM3 models, so we choose to do the comparison at the intermediate time scale of 50 years.

We show in Figure 15 responses for the AMOC and surface air temperature (the ocean heat transport response is similar to the AMOC response). The results show broad similarities between the models, with differences in the details of the amplitude and characteristics of the response. The AMOC response is broadly similar between CM2.1 and FLOR, although the CM2.1 model response at this timescale is more limited in duration than in FLOR. The shorter internal timescale for the AMOC in CM2.1 suggests that negative feedbacks associated with the oscillatory behavior kick in more rapidly, limiting the response of the AMOC in each phase of the NAO forcing. The response in FLOR to the same forcing is more persistent, consistent with the longer timescale of internal variability. The surface air temperature results are consistent with the AMOC results, with perhaps somewhat more noise in the responses (compare the temperature response in CM2.1 and FLOR to their respective AMOC responses, and it is apparent that the temperature response has more noise).

Given this spread among the models in their response to the NAO forcing, particularly for temperature, we compute a multi-model mean response to the NAO forcing, and show this in Figure 16. We see a well-defined and coherent AMOC response to the NAO forcing, with a response amplitude of approximately 2 Sv (corresponding to a 1 standard deviation change in the NAO). This corresponds to an approximately 0.2K amplitude response of extratropical NH mean surface air temperature to a one standard deviation change in the NAO. For a 50-year timescale of forcing, this implies a trend in extratropical hemispheric temperature of 0.4K/25 years.

7. Summary and Discussion

This work systematically explores the impact of interannual to centennial scale variations in the NAO on the climate system through the effect of NAO-related surface heat fluxes on the ocean. The large-scale climatic impacts arise through NAO-induced changes to the ocean that in turn modify the rest of the climate system. We have conducted suites of experiments with multiple climate models in which we artificially impose extra heat flux anomalies on the model ocean in the North Atlantic. The heat flux anomalies have the spatial structure of the NAO, but are modified such that their areal integral is zero, meaning that there is no net addition of heat to the coupled system.

In its positive phase, NAO fluxes remove heat more heat than usual from the ocean in the subpolar and subtropical North Atlantic, while removing less heat than usual from the western Atlantic and eastern Nordic Seas. The enhanced removal of heat from the subpolar gyre and Labrador Sea increases near-surface density and mixed layer depths, thereby enhancing deepwater formation and horizontal density gradients, leading to an enhanced AMOC and associated poleward oceanic heat transport (Danabasoglu et al. 2012a). By conducting simulations with multiple models in which the NAO-related fluxes are instantaneously ”switched-on” and maintained indefinitely in a positive NAO phase, we find that there is an approximate decadal-scale adjustment process in which the AMOC strengthens.

We conduct suites of experiments in which we subject the model to sinusoidally varying NAO-related fluxes, similar to Visbeck et al (1998). In simulations with NAO forcing periods ranging from 2 to 100 years, we see that the model AMOC has very little response to forcing at time scales shorter than a decade or so. The adjustment processes by which the AMOC responds to NAO forcing take of order a decade, so that forcing on shorter timescales is not able to significantly influence the AMOC. At longer timescales the AMOC varies largely in phase with the forcing, although exhibiting some preference for forcing close to the dominant timescale of internal variability (approximately 15-20 years for the CM2.1 model, and longer for the FLOR and CM3 models). The amplitude of the AMOC variations are largely independent of the timescale of forcing for timescales longer than 20 years.

The response to NAO-like atmospheric forcing has previously been studied in ocean-only models (Visbeck et al. 1998; Eden and Willebrand 2001; Eden and Jung 2001; Lohmann et al. 2009; Zhai et al. 2014) and ocean reanalyses (Huang et al. 2012), and an approximate 5-10 year timescale of the ocean's response to the NAO has also been shown. While past studies on this topic have primarily used ocean-only models, we have employed here a fully coupled ocean-atmosphere model to explore the impact of the simulated ocean changes back onto the rest of the climate system. This lagged response of the AMOC to variations of the NAO is important for interpreting the AMOC response to anthropogenic forcing (Delworth and Dixon 2000), and is an important physical underpinning for decadal prediction (Yeager et al. 2012; Yeager and Danabasoglu 2014; Hermanson et al. 2014).

The large-scale climatic response to NAO-induced AMOC variations is assessed as a function of timescale. While the amplitude of AMOC variations does not vary much as the timescale of forcing is increased from 20 years to 100 years, the amplitude of the large-scale climatic response increases substantially. At longer time scales the time-integral of the ocean heat transport variations increases, since the ocean heat transport is above (or below) normal for longer periods of time, leading to larger climatic impacts. These impacts include larger reductions (or increases) of sea ice and snow cover, which in turn increase (reduce) the impacts of albedo feedback, leading to further amplification. For example, the response of NH extratropical surface air temperature to NAO variations of the same amplitude is three times larger for the case of forcing at 100 years than at 20 years. This dependence may be a crucial factor in assessing the impact of NAO-induced AMOC variations on past climates. Similar amplification can be seen in the NAO-induced AMOC impacts on Artic sea ice and large-scale atmospheric circulation, including changes in tropical atmospheric circulation of relevance for tropical storms.

We perform identical experiments with three different models in order to test the robustness of the results. We find that the primary results are robust across the models, although details of the amplitudes of the response can vary.

These simulations focus on the response to NAO-induced surface heat flux anomalies. Preliminary experiments showed that heat flux forcing was the dominant term influencing AMOC variability at longer time scales in these models. However, it should be noted that these models all use a relatively coarse ocean model, with horizontal resolution of approximately 1^{o}. The response of a model with much finer resolution and more energetic flows could be quite different, with a potentially larger sensitivity to momentum fluxes. This is especially relevant in light of the observed AMOC weakening associated with anomalous winds in 2009-2010 (Roberts et al. 2013).

We speculate that the biases of the models used in this study will likely have some impact on their estimate of NAO-induced AMOC variability and its climatic impact (Menary et al. 2015). For example, the FLOR model has a tendency for excessive sea ice in portions of the Northern Atlantic and adjacent regions, especially in the Barents Sea. This could overestimate the impact of ice-albedo feedbacks. Similarly the albedos associated with sea ice and snow cover on sea ice in CM2.1 are perhaps on the lower end of observational estimates, thereby potentially underestimating ice-albedo feedbacks in CM2.1. Simulated NH summer sea ice in CM2.1 is also less than observed (Delworth et al. 2006), potentially reducing ice-albedo feedbacks. In addition, other biases, such as the displacement of the Gulf Stream and the lack of intense boundary currents and frontal zones, could also have some impact on the overall estimates of variability and the sensitivity to NAO-induced AMOC variability. Recent work (Vecchi et al. 2014b) has shown that reducing biases in the tropical Pacific is associated with an improved simulation of ENSO, providing support to the idea that reducing model biases could lead to improved simulation of variability.

The amplitude of the NAO forcing used in the present study is comparable to the interdecadal-scale variations observed in the NAO over the last century. The amplitude of the forcing used here corresponds to one standard deviation (a value of 1.9) of the NAO station index time series (NAO station data from https://climatedataguide.ucar.edu/climate-data/hurrell-north-atlantic-oscillation-nao-index-station-based). In the above observed NAO data set, the NAO was greater than 2.0 in the early 20th century, declined to less than -2.0 in the late 1960s, and increased to values greater than 2.0 in the 1990s. These observed interdecadal swings are comparable to the amplitude of the NAO index changes applied in this study. This suggests that variations of the NAO could have a significant impact on the AMOC and large-scale climate over the last century, including sea level in the western North Atlantic. For example, in our simulations a swing of the NAO corresponding to two standard deviations can alter NH extratropical surface air temperature by approximately 0.4K. On sufficiently long time scales this swing would also lead to substantial changes in tropical Atlantic atmospheric circulation of relevance for tropical storm formation.

One interesting aspect is that the impact of AMOC fluctuations is dependent to some extent on albedo feedback. This suggests that as the climate system warms in response to increasing greenhouse gases and Arctic sea ice and snow cover diminishes, the climatic impact of AMOC fluctuations would also be reduced. Conversely, in colder climates with more extensive sea ice, these effects could be larger.

An important aspect of the present study is that we have employed an idealized representation of the flux forcing associated with the NAO, treating the NAO as a static spatial pattern. In reality the spatial characteristics of the NAO vary over time (Hurrell and Deser 2009; Moore et al. 2013), and this could complicate the interpretation offered by our idealized framework.

The results of this study are of course limited by the fidelity of the models employed, particularly in terms of the ocean component. The models are unable to resolve oceanic mesoscale eddies or the effects of deep overflows, such as over the sills between Greenland and Iceland, or near the Faroe Banks. The model ocean itself has relatively large viscosity, resulting in weak boundary currents. In addition, the impacts of intense cyclones and their influence on air-sea interactions is missing. Nevertheless, it is likely that these models capture important relationships between the NAO, the AMOC, and larger-scale climate. These relationships are strongly influenced by oceanic adjustment to sustained changes in the NAO, involving changes in the AMOC and oceanic heat transport, and their subsequent influence on the atmosphere, including radiative feedback processes.

Acknowledgements

We wish to thank Drs. Alistair Adcroft , Yohan Ruprich-Robert, and Liping Zhang for very helpful comments on an earlier version of this manuscript.

References

Biastoch, A., C. W. Böning, J. Getzlaff, J.-M. Molines, and G. Madec, 2008: Causes of Interannual–Decadal Variability in the Meridional Overturning Circulation of the Midlatitude North Atlantic Ocean. *J. Clim.*, **21**, 6599–6615, doi:10.1175/2008JCLI2404.1.

Bindoff, N. L., and Coauthors, 2013: Detection and Attribution of Climate Change: from Global to Regional. *Contribution of Working Group I to the Fifth Assessment Report of the Intergovernmental Panel on Climate Change*, Cambridge University Press, Cambridge, United Kingdom and New York, NY, USA.

Bjerknes, J., 1964: Atlantic Air-Sea Interaction. *Advancs in Geophysics.*, Vol. 10 of *Advances in Geophysics.*, Academic Press, Inc., New York, USA, 1–82.

Chylek, P., C. K. Folland, G. Lesins, M. K. Dubey, and M. Wang, 2009: Arctic air temperature change amplification and the Atlantic Multidecadal Oscillation. *Geophys. Res. Lett.*, **36**, doi:10.1029/2009GL038777. http://doi.wiley.com/10.1029/2009GL038777 (Accessed May 29, 2015).

Cullen, H. M., A. Kaplan, P. A. Arkin, and P. B. Demenocal, 2002: Impact of the North Atlantic Oscillation on Middle Eastern climate and streamflow. *Clim. Change*, **55**, 315–338.

Danabasoglu, G., S. G. Yeager, Y.-O. Kwon, J. J. Tribbia, A. S. Phillips, and J. W. Hurrell, 2012a: Variability of the Atlantic Meridional Overturning Circulation in CCSM4. *J. Clim.*, **25**, 5153–5172, doi:10.1175/JCLI-D-11-00463.1.

——, ——, ——, ——, ——, and ——, 2012b: Variability of the Atlantic Meridional Overturning Circulation in CCSM4. *J. Clim.*, **25**, 5153–5172, doi:10.1175/JCLI-D-11-00463.1.

Dee, D. P., and Coauthors, 2011: The ERA-Interim reanalysis: configuration and performance of the data assimilation system. *Q. J. R. Meteorol. Soc.*, **137**, 553–597, doi:10.1002/qj.828.

Delworth, T. L., and K. W. Dixon, 2000: Implications of the recent trend in the Arctic/North Atlantic Oscillation for the North Atlantic thermohaline circulation. *J. Clim.*, **13**, 3721–3727.

——, and R. J. Greatbatch, 2000: Multidecadal thermohaline circulation variability driven by atmospheric surface flux forcing. *J. Clim.*, **13**, 1481–1495.

——, and M. E. Mann, 2000: Observed and simulated multidecadal variability in the Northern Hemisphere. *Clim. Dyn.*, **16**, 661–676.

——, S. Manabe, and R. J. Stouffer, 1993: Interdecadal variations of the Thermohaline Circulation in a Coupled Ocean-Atmosphere Model. *J. Clim.*, **6**, 1993–2011.

——, and Coauthors, 2006: GFDL's CM2 global coupled climate models. Part I: Formulation and simulation characteristics. *J. Clim.*, **19**.

Donner, L. J., and Coauthors, 2011: The Dynamical Core, Physical Parameterizations, and Basic Simulation Characteristics of the Atmospheric Component AM3 of the GFDL Global Coupled Model CM3. *J. Clim.*, **24**, 3484–3519, doi:10.1175/2011JCLI3955.1.

Eden, C., and T. Jung, 2001: North Atlantic interdecadal variability: oceanic response to the North Atlantic Oscillation (1865-1997). *J. Clim.*, **14**, 676–691.

——, and J. Willebrand, 2001: Mechanism of interannual to decadal variability of the North Atlantic circulation. *J. Clim.*, **14**, 2266–2280.

Frankcombe, L. M., A. von der Heydt, and H. A. Dijkstra, 2010: North Atlantic Multidecadal Climate Variability: An Investigation of Dominant Time Scales and Processes. *J. Clim.*, **23**, 3626–3638, doi:10.1175/2010JCLI3471.1.

Frankignoul, C., G. Gastineau, and Y.-O. Kwon, 2013: The Influence of the AMOC Variability on the Atmosphere in CCSM3. *J. Clim.*, **26**, 9774–9790, doi:10.1175/JCLI-D-12-00862.1.

Frierson, D. M. W., and Coauthors, 2013: Contribution of ocean overturning circulation to tropical rainfall peak in the Northern Hemisphere. *Nat. Geosci.*, **6**, 940–944, doi:10.1038/ngeo1987.

Gámiz-Fortis, S. R., 2002: Spectral characteristics and predictability of the NAO assessed through Singular Spectral Analysis. *J. Geophys. Res.*, **107**, doi:10.1029/2001JD001436. http://doi.wiley.com/10.1029/2001JD001436 (Accessed November 4, 2015).

Gerber, E. P., and G. K. Vallis, 2009: On the Zonal Structure of the North Atlantic Oscillation and Annular Modes. *J. Atmospheric Sci.*, **66**, 332–352, doi:10.1175/2008JAS2682.1.

Goddard, P. B., J. Yin, S. M. Griffies, and S. Zhang, 2015: An extreme event of sea-level rise along the Northeast coast of North America in 2009–2010. *Nat. Commun.*, **6**, 6346, doi:10.1038/ncomms7346.

Griffies, S. M., and Coauthors, 2011: The GFDL CM3 Coupled Climate Model: Characteristics of the Ocean and Sea Ice Simulations. *J. Clim.*, **24**, 3520–3544, doi:10.1175/2011JCLI3964.1.

Hermanson, L., R. Eade, N. H. Robinson, N. J. Dunstone, M. B. Andrews, J. R. Knight, A. A. Scaife, and D. M. Smith, 2014: Forecast cooling of the Atlantic subpolar gyre and associated impacts. *Geophys. Res. Lett.*, **41**, 5167–5174, doi:10.1002/2014GL060420.

Huang, B., Y. Xue, A. Kumar, and D. W. Behringer, 2012: AMOC variations in 1979–2008 simulated by NCEP operational ocean data assimilation system. *Clim. Dyn.*, **38**, 513–525, doi:10.1007/s00382-011-1035-z.

Hurrell, J., 1996: Influence of variations in extratropical wintertime teleconnections on Northern Hemisphere temperature. *Geophys. Res. Lett.*, **23**, 665–668.

Hurrell, J. W., 1995: Decadal Trends in the North Atlantic Oscillation: Regional Temperatures and Precipitation. *Science*, **269**, 676–679, doi:10.1126/science.269.5224.676.

——, and C. Deser, 2009: North Atlantic climate variability: The role of the North Atlantic Oscillation. *J. Mar. Syst.*, **78**, 28–41, doi:10.1016/j.jmarsys.2008.11.026.

Knight, J. R., R. Allan, C. K. Folland, M. Vellinga, and M. E. Mann, 2005: A signature of persistent natural thermohaline circulation cycles in observed climate. *Geophys. Res. Lett.*, **32**, doi:10.1029/2005GL024233. http://doi.wiley.com/10.1029/2005GL024233 (Accessed April 28, 2015).

Kuhlbrodt, T., A. Griesel, M. Montoya, A. Levermann, M. Hofmann, and S. Rahmstorf, 2007: On the driving processes of the Atlantic meridional overturning circulation. *Rev. Geophys.*, **45**, doi:10.1029/2004RG000166. http://doi.wiley.com/10.1029/2004RG000166 (Accessed April 7, 2015).

Kwon, Y.-O., and C. Frankignoul, 2012: Stochastically-driven multidecadal variability of the Atlantic meridional overturning circulation in CCSM3. *Clim. Dyn.*, **38**, 859–876, doi:10.1007/s00382-011-1040-2.

Li, J., C. Sun, and F.-F. Jin, 2013: NAO implicated as a predictor of Northern Hemisphere mean temperature multidecadal variability. *Geophys. Res. Lett.*, **40**, 5497–5502, doi:10.1002/2013GL057877.

Lohmann, K., H. Drange, and M. Bentsen, 2009: Response of the North Atlantic subpolar gyre to persistent North Atlantic oscillation like forcing. *Clim. Dyn.*, **32**, 273–285, doi:10.1007/s00382-008-0467-6.

McCarthy, G. D., I. D. Haigh, J. J.-M. Hirschi, J. P. Grist, and D. A. Smeed, 2015: Ocean impact on decadal Atlantic climate variability revealed by sea-level observations. *Nature*, **521**, 508–510, doi:10.1038/nature14491.

Medhaug, I., H. R. Langehaug, T. Eldevik, T. Furevik, and M. Bentsen, 2012: Mechanisms for decadal scale variability in a simulated Atlantic meridional overturning circulation. *Clim. Dyn.*, **39**, 77–93, doi:10.1007/s00382-011-1124-z.

Menary, M. B., W. Park, K. Lohmann, M. Vellinga, M. D. Palmer, M. Latif, and J. H. Jungclaus, 2012: A multimodel comparison of centennial Atlantic meridional overturning circulation variability. *Clim. Dyn.*, **38**, 2377–2388, doi:10.1007/s00382-011-1172-4.

——, D. L. R. Hodson, J. I. Robson, R. T. Sutton, R. A. Wood, and J. A. Hunt, 2015: Exploring the impact of CMIP5 model biases on the simulation of North Atlantic decadal variability: CMIP5 BIASES AFFECT VARIABILITY. *Geophys. Res. Lett.*, **42**, 5926–5934, doi:10.1002/2015GL064360.

Milly, P. C. D., and Coauthors, 2014: An Enhanced Model of Land Water and Energy for Global Hydrologic and Earth-System Studies. *J. Hydrometeorol.*, **15**, 1739–1761, doi:10.1175/JHM-D-13-0162.1.

Moore, G. W. K., I. A. Renfrew, and R. S. Pickart, 2013: Multidecadal Mobility of the North Atlantic Oscillation. *J. Clim.*, **26**, 2453–2466, doi:10.1175/JCLI-D-12-00023.1.

Park, W., and M. Latif, 2008: Multidecadal and multicentennial variability of the meridional overturning circulation. *Geophys. Res. Lett.*, **35**, doi:10.1029/2008GL035779. http://doi.wiley.com/10.1029/2008GL035779 (Accessed April 28, 2015).

Roberts, C. D., and Coauthors, 2013: Atmosphere drives recent interannual variability of the Atlantic meridional overturning circulation at 26.5°N: ATMOSPHERE DRIVES AMOC VARIABILITY. *Geophys. Res. Lett.*, **40**, 5164–5170, doi:10.1002/grl.50930.

Scaife, A. A., C. K. Folland, L. V. Alexander, A. Moberg, and J. R. Knight, 2008: European Climate Extremes and the North Atlantic Oscillation. *J. Clim.*, **21**, 72–83, doi:10.1175/2007JCLI1631.1.

Shaffrey, L., and R. Sutton, 2006: Bjerknes compensation and the decadal variability of the energy transports in a coupled climate model. *J. Clim.*, **19**, 1167–1181.

Steinman, B. A., M. E. Mann, and S. K. Miller, 2015: Atlantic and Pacific multidecadal oscillations and Northern Hemisphere temperatures. *Science*, **347**, 988–991, doi:10.1126/science.1257856.

Sutton, R., and D. Hodson, 2005: Atlantic Ocean Forcing of North American and European Summer Climate. *Science*, **309**, 115–118.

Sutton, R. T., and B. Dong, 2012: Atlantic Ocean influence on a shift in European climate in the 1990s. *Nat. Geosci.*, **5**, 788–792, doi:10.1038/ngeo1595.

Trigo, R. M., T. J. Osborn, and J. M. Corte-Real, 2002: The North Atlantic Oscillation influence on Europe: climate impacts and associated physical mechanisms. *Clim. Res.*, **20**, 9–17.

Tulloch, R., and J. Marshall, 2012: Exploring Mechanisms of Variability and Predictability of Atlantic Meridional Overturning Circulation in Two Coupled Climate Models. *J. Clim.*, **25**, 4067–4080, doi:10.1175/JCLI-D-11-00460.1.

Vecchi, G. A., and Coauthors, 2014a: On the Seasonal Forecasting of Regional Tropical Cyclone Activity. *J. Clim.*, **27**, 7994–8016, doi:10.1175/JCLI-D-14-00158.1.

——, and Coauthors, 2014b: On the Seasonal Forecasting of Regional Tropical Cyclone Activity. *J. Clim.*, **27**, 7994–8016, doi:10.1175/JCLI-D-14-00158.1.

Vellinga, M., and P. Wu, 2004: Low-latitude freshwater influence on centennial variability of the Atlantic thermohaline circulation. *J. Clim.*, **17**, 4498–4511.

Visbeck, M., H. Cullen, G. Krahmann, and N. Naik, 1998: An ocean model's response to North Atlantic Oscillation-like wind forcing. *Geophys. Res. Lett.*, **25**, 4521–4524.

Wunsch, C., 1999: The interpretation of short climate records, with comments on the North Atlantic and Southern Oscillations. *Bull. Am. Meteorol. Soc.*, **80**, 245–255.

Yang, H., Y. Wang, and Z. Liu, 2013: A modelling study of the Bjerknes compensation in the meridional heat transport in a freshening ocean. *Tellus A*, **65**, doi:10.3402/tellusa.v65i0.18480. http://www.tellusa.net/index.php/tellusa/article/view/18480 (Accessed September 21, 2015).

Yeager, S., and G. Danabasoglu, 2012: Sensitivity of Atlantic Meridional Overturning Circulation Variability to Parameterized Nordic Sea Overflows in CCSM4. *J. Clim.*, **25**, 2077–2103, doi:10.1175/JCLI-D-11-00149.1.

——, and ——, 2014: The Origins of Late-Twentieth-Century Variations in the Large-Scale North Atlantic Circulation. *J. Clim.*, **27**, 3222–3247, doi:10.1175/JCLI-D-13-00125.1.

——, A. Karspeck, G. Danabasoglu, J. Tribbia, and H. Teng, 2012: A Decadal Prediction Case Study: Late Twentieth-Century North Atlantic Ocean Heat Content. *J. Clim.*, **25**, 5173–5189, doi:10.1175/JCLI-D-11-00595.1.

Zhai, X., H. L. Johnson, and D. P. Marshall, 2014: A Simple Model of the Response of the Atlantic to the North Atlantic Oscillation. *J. Clim.*, **27**, 4052–4069, doi:10.1175/JCLI-D-13-00330.1.

Zhang, R., and T. L. Delworth, 2005: Simulated tropical response to a substantial weakening of the Atlantic thermohaline circulation. *J. Clim.*, **18**, 1853–1860.

——, and G. K. Vallis, 2007: The Role of Bottom Vortex Stretching on the Path of the North Atlantic Western Boundary Current and on the Northern Recirculation Gyre. *J. Phys. Oceanogr.*, **37**, 2053–2080, doi:10.1175/JPO3102.1.

——, T. L. Delworth, and I. M. Held, 2007: Can the Atlantic Ocean drive the observed multidecadal variability in Northern Hemisphere mean temperature? *Geophys. Res. Lett.*, **34**, doi:10.1029/2006GL028683. http://doi.wiley.com/10.1029/2006GL028683 (Accessed May 29, 2015).

Zhu, X., and J. Jungclaus, 2008: Interdecadal variability of the meridional overturning circulation as an ocean internal mode. *Clim. Dyn.*, **31**, 731–741, doi:10.1007/s00382-008-0383-9.

Figures

Figure 1 Spatial pattern of the heat flux anomalies (W m^{-2}) used as anomalous flux forcings in the model experiments. Negative values mean a flux of heat from the ocean to the atmosphere. The fluxes in (a) are derived from the ECMWF-Interim reanalysis, and are the mean fluxes over Dec-March that correspond to a one standard deviation anomaly of the North Atlantic Oscillation. The fluxes in (b) are from a long control simulation of the CM2.1 model, and also correspond to a one standard deviation anomaly of the North Atlantic Oscillation.

Figure 2 (a)-(c) Streamfunction of zonal mean Atlantic ocean circulation from various model (units are Sverdrups; $Sv = 10^6$ m^3s^{-1}), denoting the mean AMOC in each model. (a) CM2.1, (b) FLOR, and (c) CM3. The flow is along the lines of the streamfunction, with the flow speed proportional to the gradient of the streamfunction. Flow is clockwise around a streamfunction maximum in the latitude-depth plane. (d) Time series of the AMOC index from each simulation, calculated as the maximum value of the streamfunction each year over 20°N-65°N. Black is CM2.1, red is FLOR, and green is CM3. (e) Spectra of the time series of AMOC amplitude in the three models. Black indicates CM2.1, red indicates FLOR, and green indicates CM3. For each model the thick line represents the spectral estimates, the thin solid line is a red noise (first order Markov process) spectrum fitted to the model spectrum, and the dashed lines represent 95% confidence interval above the red noise spectrum. The units are frequency along the bottom x-axis (cycles yr^{-1}) and period in years along the top x-axis. The units along the y-axis are spectral density.

Figure 3 Ensemble mean response of the AMOC in the CM2.1 model to the switch-on of NAO-related surface heat fluxes in the North Atlantic. The NAO fluxes are switched on at time 0. The quantity plotted is the maximum streamfunction at 45°N in the experiment with the NAO forcing minus the control simulation.

Figure 4 Adjustment of the North Atlantic in CM2.1 to a sudden switch on of heat flux anomaly corresponding to a one standard deviation increase of the North Atlantic Oscillation. Top row:

Climatological mean fields for various quantities as noted by labels at the top of each column. Rows 2-5: anomalies at various times after the switch on of the NAO heat flux. The time is shown on the right, and indicates how much time has passed since the switch on of the NAO-related heat flux forcing. The variables are listed along the top, so that each column corresponds to one variable. Units: mixed layer depth in m., AMOC in Sverdrups, heat transport in units of 10^{13}W, SST in ^{o}C, and sea surface salinity (SSS) in Practical Salinity Units (PSU).

Figure 5 Time series of AMOC index (defined as the maximum streamfunction value each year over the domain 20^{o}N-65^{o}N) for various experiments using the CM2.1 model. The red curve in each panel shows values from the reference control simulation, calculated as the ensemble mean over ten segments of the control simulation that correspond to the ten ensemble members of the perturbation experiments. (a) Black (blue) curve shows 10-member ensemble mean AMOC from simulations with NAO forcing at a timescale of 2 (5) years. (b) Black (blue) curve shows 10-member ensemble mean AMOC from simulations with NAO forcing at a timescale of 10 (20) years. (c) Black (blue) curve shows 10-member ensemble mean AMOC from simulations with NAO forcing at a timescale of 50 (100) years.

Figure 6 (a) Each circle represents the standard deviation of the ensemble mean AMOC time series from a perturbation experiment using NAO forcing at a particular timescale. The values along the y-axis indicate the value of the standard deviation, while the values along the x-axis indicate the timescale (in years) of the NAO forcing for each experiment. (b) Same as (a) for meridional ocean heat transport at 23^{o}N (summed over all longitudes, units are 10^{15} W). (c) Same as (a) for annual mean surface air temperature (units are K) averaged over all points poleward of 23^{o}N. (d) Same as (a) for annual mean sea ice thickness averaged over all points poleward of 55^{o}N, units are cm. (e) Same as (a) for air-sea surface heat flux averaged over all points poleward of 23^{o}N, units are W m^{-2}. (f) Same as (a) for net upward shortwave radiation at the top of the atmosphere, averaged over all points poleward of 23^{o}N, units are W m^{-2}.

Figure 7 Time series of various quantities in model simulations driven by a periodic NAO heat flux forcing. In each panel we show the results from a 20-year timescale NAO forcing experiment (black) and a 100-year timescale NAO forcing (red). Each time series is the 10-member ensemble mean of the NAO forced experiment minus the corresponding control simulation. The 20-year (100-year) forcing experiments are 100 (200) years in duration. (a) AMOC index, units are Sv. (b) Meridional ocean heat transport at 23^{o}N, units are 10^{15} W. (c) Surface air temperature, averaged over all points poleward of 23^{o}N, units are K. (d) Annual mean sea ice thickness, averaged over all points poleward of 55^{o}N, units are cm. (e) Annual mean net upward shortwave radiation at the top of the atmosphere (W m^{-2}), averaged over all points poleward of 23^{o}N. (f) Ocean-atmosphere heat flux (W m^{-2}), averaged over all points poleward of 23^{o}N.

Figure 8 (a) Regression of time series of imposed NAO forcing versus itself. (b) Regression of changes in oceanic (Atlantic only) and atmospheric (all longitudes) heat transport at 50^{o}N versus the NAO forcing. Time is along the x-axis in years. Negative (positive) values indicate years before (after) the imposed NAO maximum. Units are 10^{14} J (a value of +1.0 would indicate an enhanced poleward oceanic heat transport of 10^{14} J). Thick red line is for total poleward oceanic heat transport, thin red line for the meridional overturning component (moc) of the transport, and dashed line for the gyre component of the transport. Blue line is poleward atmospheric heat transport at 50^{o}N. (c) Regression of changes in net incoming radiation at the top of the atmosphere versus the NAO time series, integrated over all regions poleward of 50°N. Positive values indicate an increase in the flux of radiation from space to Earth (ie, a heating of the climate system). Red denotes net shortwave radiation, blue denotes longwave radiation, black denotes the net radiative flux. Units are 10^{14} J. For example, negative values of longwave radiation for years 0 to 30 after the NAO forcing indicate an increase of outgoing longwave radiation to space as a response to warming of the Northern Hemisphere associated with the increased poleward oceanic heat transport shown in (b).

Figure 9 Spatial patterns of simulated response to NAO-related surface heat flux anomalies. The responses are averaged over the months of Jan-Mar. Left (right) column shows results from simulations with 20-year (100-year) NAO forcing. Values plotted are regression coefficients of the various fields versus the imposed NAO time series, normalized to represent the response to a two standard deviation change in the NAO. Left column are results for a 20-year timescale of flux forcing, showing fields 7 years after maximum of imposed NAO flux forcing. The right column shows results for a 100-year timescale of flux forcing, plotted 13 years after maximum of imposed NAO flux forcing.

Figure 10 Same as Figure 9, but for sea ice thickness. Units are meters per two standard deviation NAO forcing.

Figure 11 Spatial patterns of simulated response to an increase in the AMOC induced by NAO-related surface heat flux anomalies. The responses are averaged over the months of Jul-Sep. Left (right) column shows results from simulations with 20-year (100-year) NAO forcing. Values plotted are regression coefficients of the various fields versus the time series of the heat flux forcing; these are normalized to represent the response to a two standard deviation change in the NAO-induced fluxes. Left column are results for a 20-year timescale of flux forcing, showing fields 7 years after maximum of imposed NAO flux forcing. The right column shows results for a 100-year timescale of flux forcing, plotted 13 years after maximum of imposed NAO flux forcing. The vertical shear of the zonal wind (bottom row) is calculated as the zonal wind at 250 hPa minus the zonal wind at 850 hPa.

Figure 12 Same as Figure 11, but for sea ice thickness. Units are meters per two standard deviation NAO forcing.

Figure 13 Regression of annual mean sea level height anomaly versus the time series of NAO forcing, expressed as the difference in cm between a positive one standard deviation NAO forcing and a negative one standard deviation NAO forcing. For both cases the maps are representative of conditions 6 years after the maximum NAO flux forcing. (a) Case with NAO-forcing at 20 years. (b) Case with NAO-forcing at 100 years.

Figure 14 Response of AMOC (left column) and zonally averaged surface air temperature (right column) to sudden switch on of NAO related heat flux forcing. Top row is from CM2.1, middle row from FLOR, and bottom row from CM3. Units are Sv for AMOC changes, and K for temperature changes. Time is listed along the x-axis in years, latitude is on the y-axis.

Figure 15 Response of AMOC (left column) and zonally averaged surface air temperature (right column) to sinusoidal NAO heat flux forcing with amplitude of one standard deviation of the NAO time series and period of 50 years. Top row is from CM2.1, middle row from FLOR, and bottom row from CM3. Units are Sv for AMOC changes, and K for temperature changes. Time is listed along the x-axis in years, and latitude along the y-axis.

Figure 16 Response to 50-year NAO heat flux forcing calculated as the ensemble mean response from CM2.1, FLOR, and CM3. We first calculate the ensemble mean using each model, and then compute the mean of those three ensemble means. Time is listed in years along the x-axis, indicating years since switching on the NAO-related heat fluxes. (a) AMOC response as a function of latitude and time, units are Sv. (b) NH mean surface air temperature response, averaged over the domain 23^{o}N-90^{o}N. Units are K.

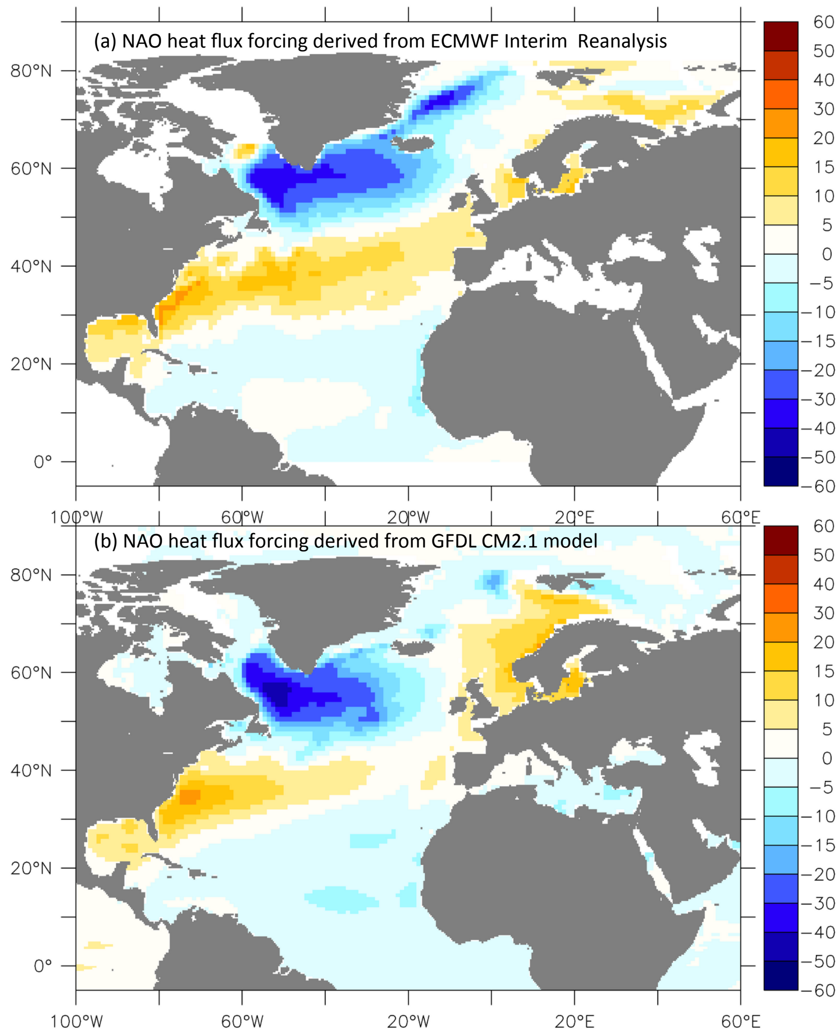

Figure 1 Spatial pattern of the heat flux anomalies (W m^{-2}) used as anomalous flux forcings in the model experiments. Negative values mean a flux of heat from the ocean to the atmosphere. The fluxes in (a) are derived from the ECMWF-Interim reanalysis, and are the mean fluxes over Dec-March that correspond to a one standard deviation anomaly of the North Atlantic Oscillation. The fluxes in (b) are from a long control simulation of the CM2.1 model, and also correspond to a one standard deviation anomaly of the North Atlantic Oscillation.

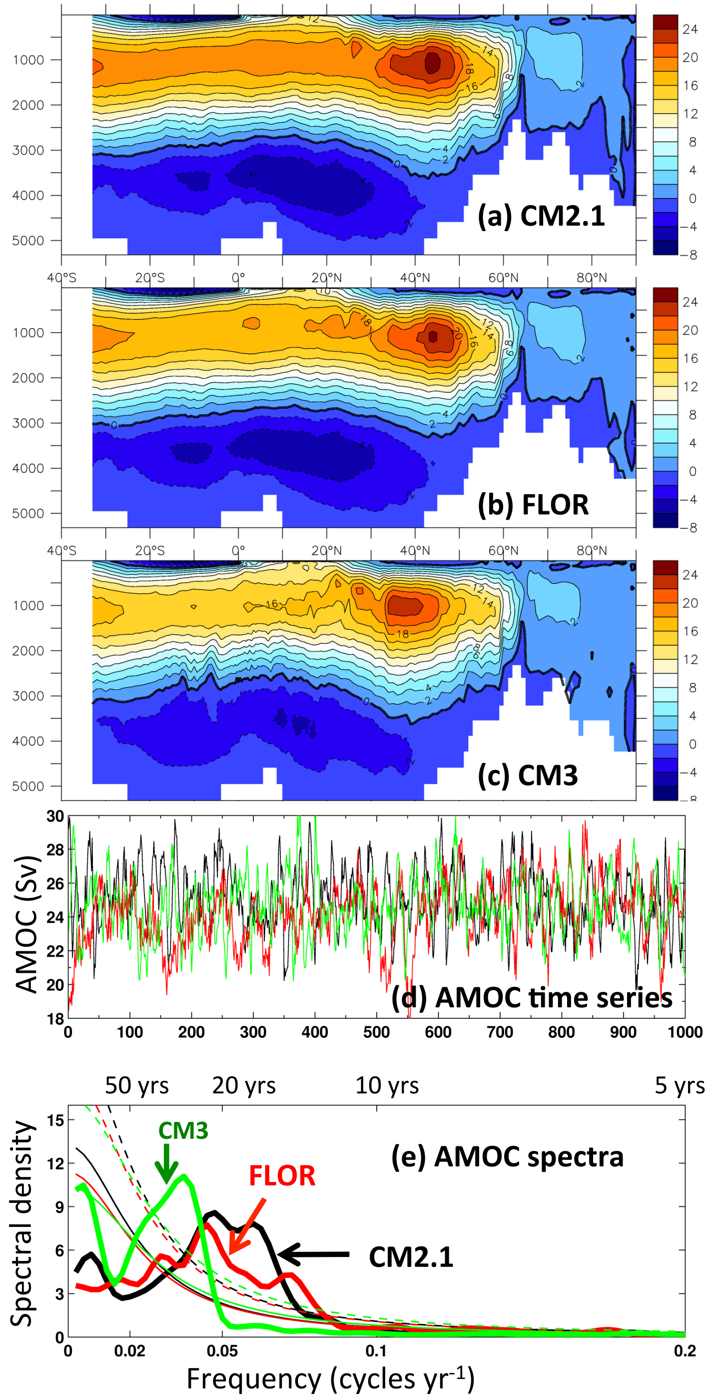

Figure 2 (a)-(c) Streamfunction of zonal mean Atlantic ocean circulation from various model (units are Sverdrups; Sv = 10^6 m^3s^{-1}), denoting the mean AMOC in each model. (a) CM2.1, (b) FLOR, and (c) CM3. The flow is along the lines of the streamfunction, with the flow speed proportional to the gradient of the streamfunction. Flow is clockwise around a streamfunction maximum in the latitude-depth plane. (d) Time series of the AMOC index from each simulation, calculated as the maximum value of the streamfunction each year over 20°N-65°N. Black is CM2.1, red is FLOR, and green is CM3. (e) Spectra of the time series of AMOC amplitude in the three models. Black indicates CM2.1, red indicates FLOR, and green indicates CM3. For each model the thick line represents the spectral estimates, the thin solid line is a red noise (first order Markov process) spectrum fitted to the model spectrum, and the dashed lines represent 95% confidence interval above the red noise spectrum. The units are frequency along the bottom x-axis (cycles yr^{-1}) and period in years along the top x-axis. The units along the y-axis are spectral density.

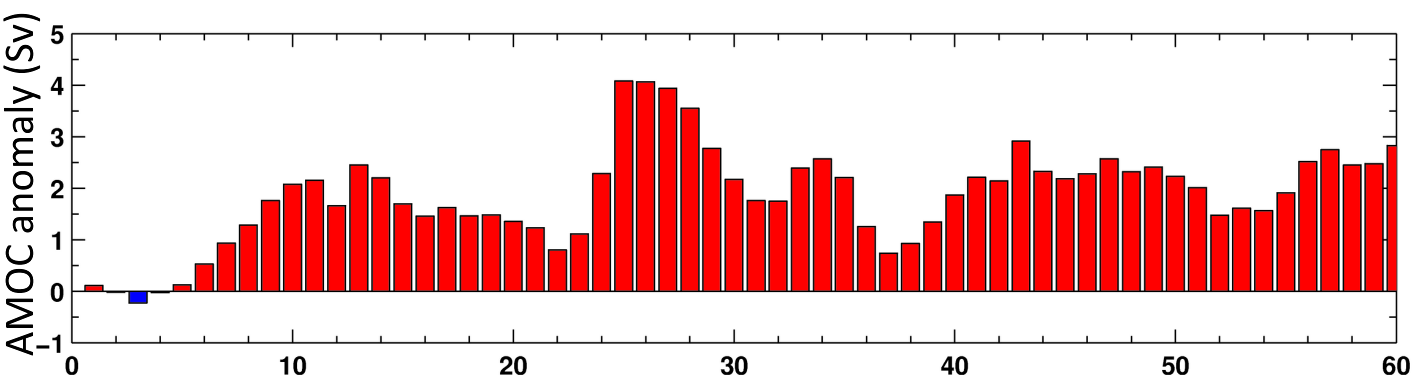

Figure 3 Ensemble mean response of the AMOC in the CM2.1 model to the switch-on of NAO-related surface heat fluxes in the North Atlantic. The NAO fluxes are switched on at time 0. The quantity plotted is the maximum streamfunction at 45°N in the experiment with the NAO forcing minus the control simulation.

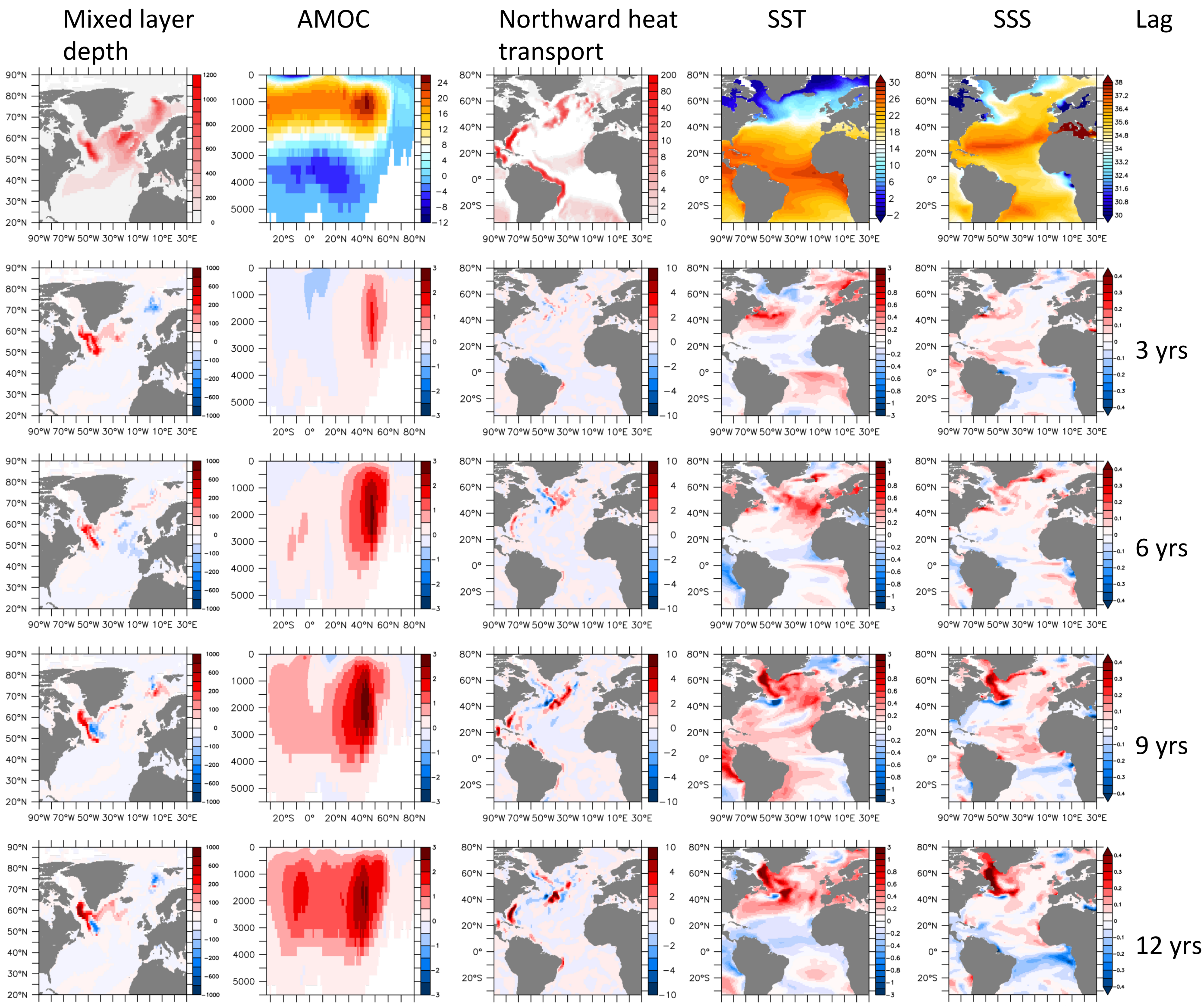

Figure 4 Adjustment of the North Atlantic in CM2.1 to a sudden switch on of heat flux anomaly corresponding to a one standard deviation increase of the North Atlantic Oscillation. Top row: Climatological mean fields for various quantities as noted by labels at the top of each column. Rows 2-5: anomalies at various times after the switch on of the NAO heat flux. The time is shown on the right, and indicates how much time has passed since the switch on of the NAO-related heat flux forcing. The variables are listed along the top, so that each column corresponds to one variable. Units: mixed layer depth in m., AMOC in Sverdrups, heat transport in units of 10^{13}W, SST in ^{o}C, and sea surface salinity (SSS) in Practical Salinity Units (PSU).

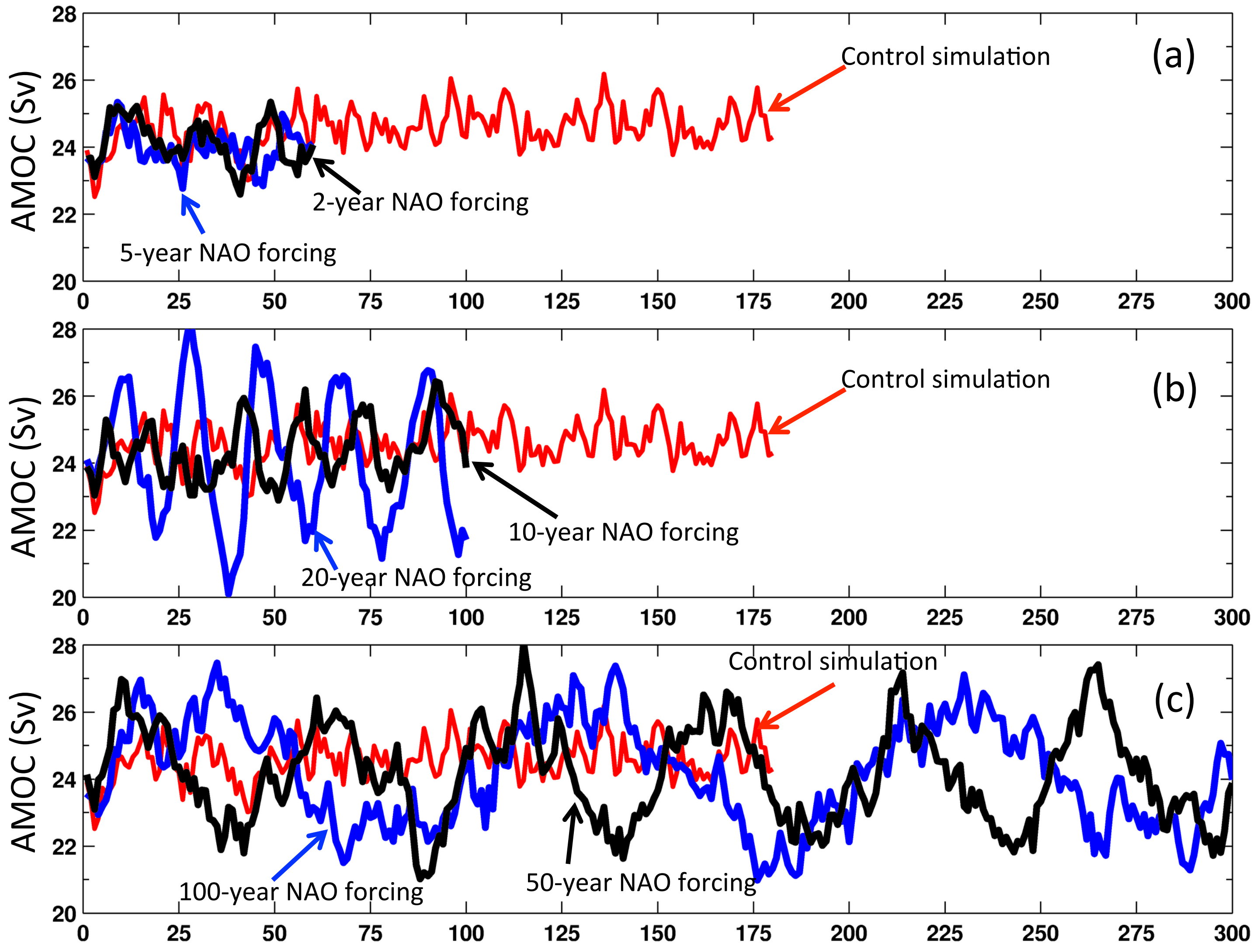

Figure 5 Time series of AMOC index (defined as the maximum streamfunction value each year over the domain 20°N-65°N) for various experiments using the CM2.1 model. The red curve in each panel shows values from the reference control simulation, calculated as the ensemble mean over ten segments of the control simulation that correspond to the ten ensemble members of the perturbation experiments. (a) Black (blue) curve shows 10-member ensemble mean AMOC from simulations with NAO forcing at a timescale of 2 (5) years. (b) Black (blue) curve shows 10-member ensemble mean AMOC from simulations with NAO forcing at a timescale of 10 (20) years. (c) Black (blue) curve shows 10-member ensemble mean AMOC from simulations with NAO forcing at a timescale of 50 (100) years.

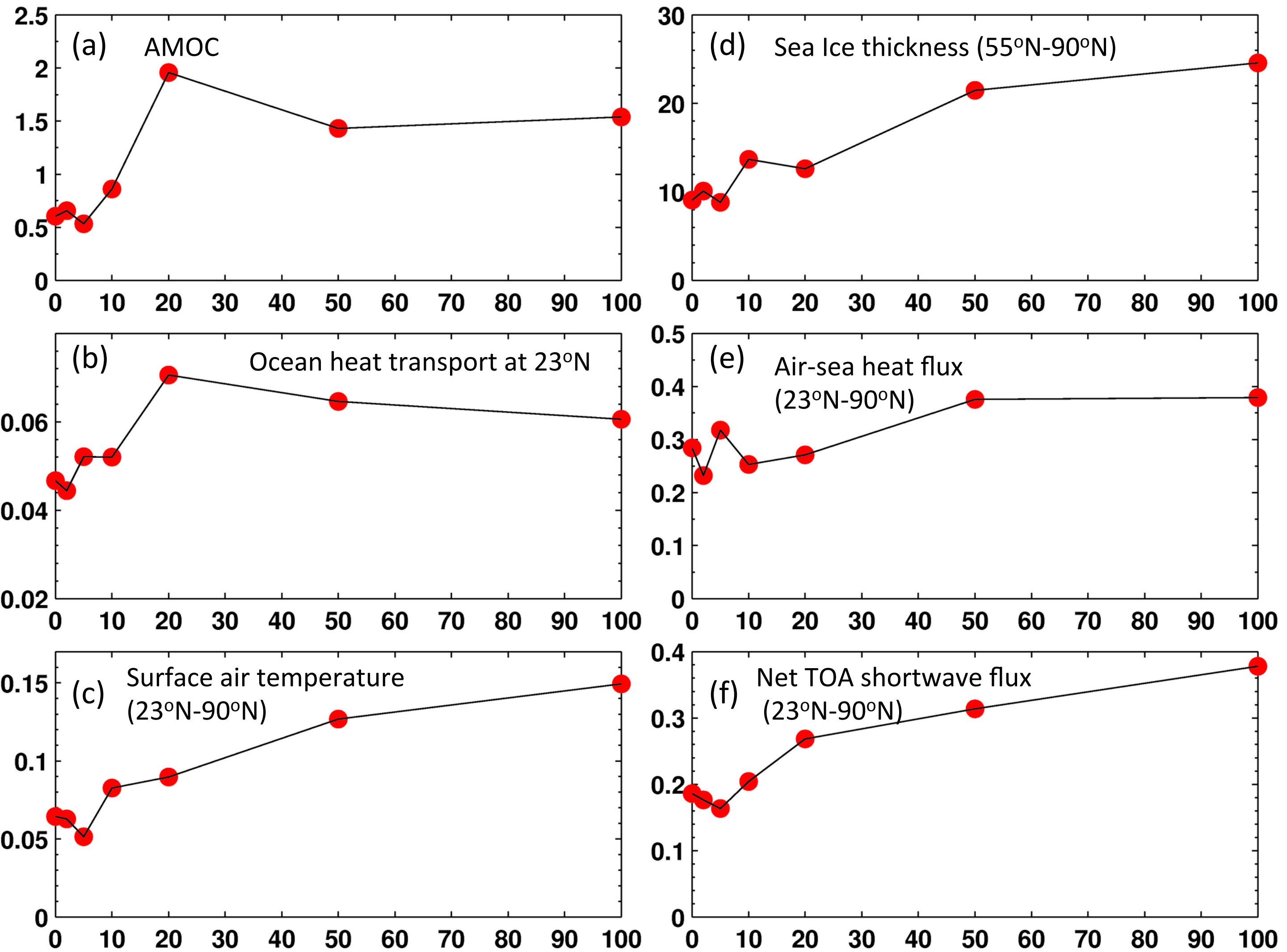

Figure 6 (a) Each circle represents the standard deviation of the ensemble mean AMOC time series from a perturbation experiment using NAO forcing at a particular timescale. The values along the y-axis indicate the value of the standard deviation, while the values along the x-axis indicate the timescale (in years) of the NAO forcing for each experiment. (b) Same as (a) for meridional ocean heat transport at 23°N (summed over all longitudes, units are 10^{15} W). (c) Same as (a) for annual mean surface air temperature (units are K) averaged over all points poleward of 23°N. (d) Same as (a) for annual mean sea ice thickness averaged over all points poleward of 55°N, units are cm. (e) Same as (a) for air-sea surface heat flux averaged over all points poleward of 23°N, units are W m^{-2}. (f) Same as (a) for net upward shortwave radiation at the top of the atmosphere, averaged over all points poleward of 23°N, units are W m^{-2}.

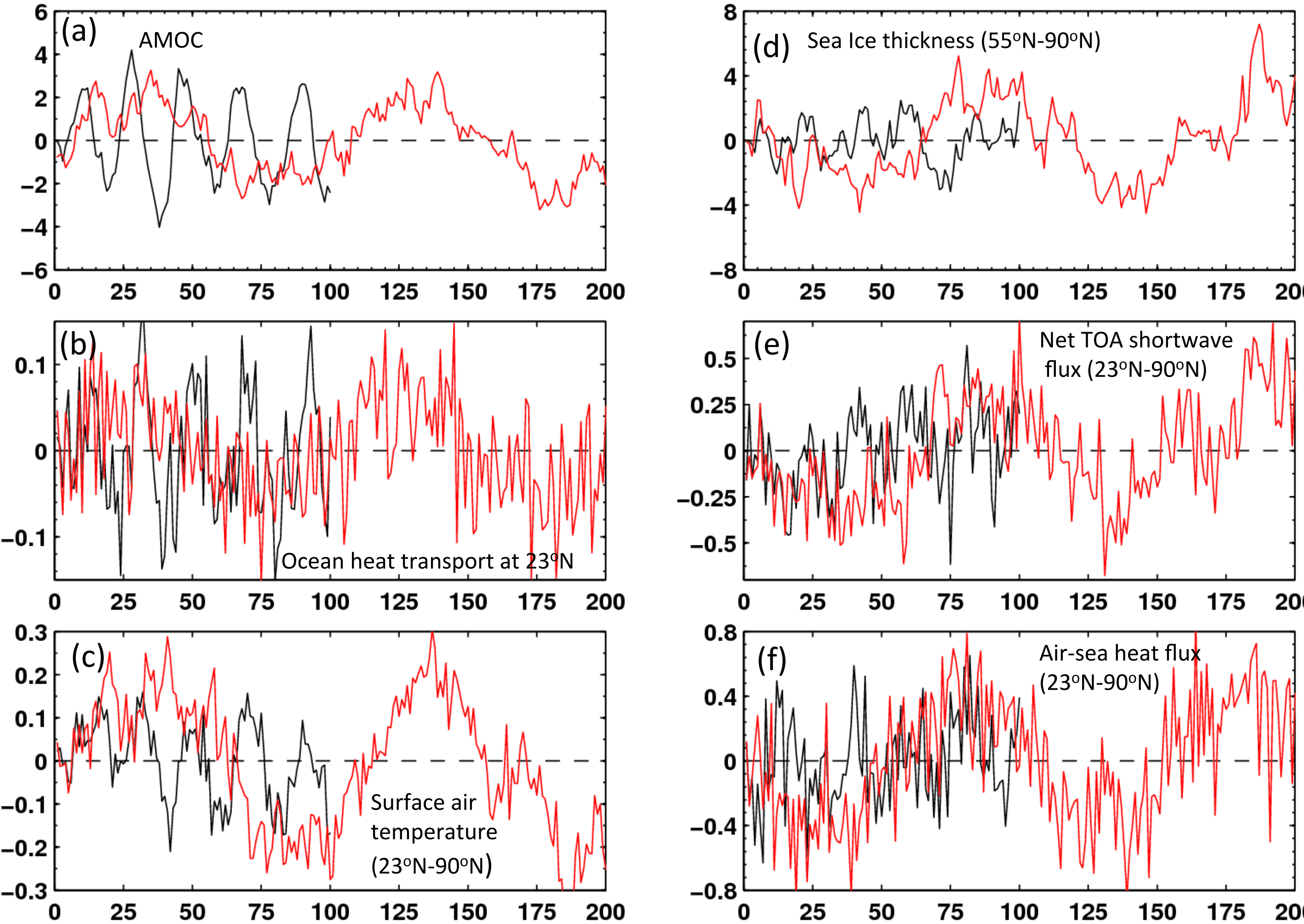

Figure 7 Time series of various quantities in model simulations driven by a periodic NAO heat flux forcing. In each panel we show the results from a 20-year timescale NAO forcing experiment (black) and a 100-year timescale NAO forcing (red). Each time series is the 10-member ensemble mean of the NAO forced experiment minus the corresponding control simulation. The 20-year (100-year) forcing experiments are 100 (300) years in duration. (a) AMOC index, units are Sv. (b) Meridional ocean heat transport at 23°N, units are 10^{15} W. (c) Surface air temperature, averaged over all points poleward of 23°N, units are K. (d) Annual mean sea ice thickness, averaged over all points poleward of 55°N, units are cm. (e) Annual mean net upward shortwave radiation at the top of the atmosphere (W m^{-2}), averaged over all points poleward of 23°N. (f) Ocean-atmosphere heat flux (W m^{-2}), averaged over all points poleward of 23°N.

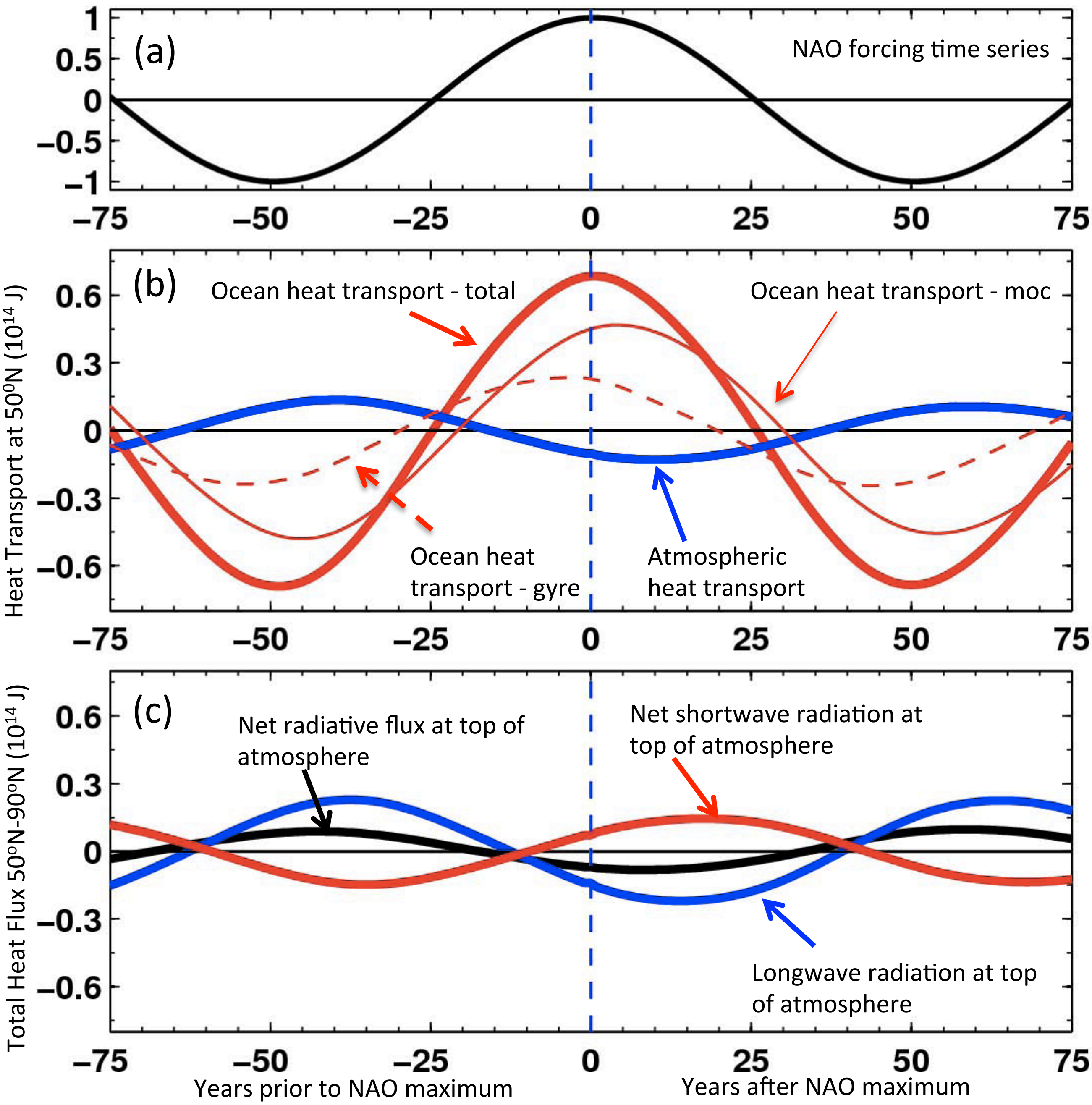

Figure 8 (a) Regression of time series of imposed NAO forcing versus itself. (b) Regression of changes in oceanic (Atlantic only) and atmospheric (all longitudes) heat transport at 50°N versus the NAO forcing. Time is along the x-axis in years. Negative (positive) values indicate years before (after) the imposed NAO maximum. Units are 10^{14} J (a value of +1.0 would indicate an enhanced poleward oceanic heat transport of 10^{14} J). Thick red line is for total poleward oceanic heat transport, thin red line for the meridional overturning component (moc) of the transport, and dashed line for the gyre component of the transport. Blue line is poleward atmospheric heat transport at 50°N. (c) Regression of changes in net incoming radiation at the top of the atmosphere versus the NAO time series, integrated over all regions poleward of 50°N. Positive values indicate an increase in the flux of radiation from space to Earth (ie, a heating of the climate system). Red denotes net shortwave radiation, blue denotes longwave radiation, black denotes the net radiative flux. Units are 10^{14} J. For example, negative values of longwave radiation for years 0 to 30 after the NAO forcing indicate an increase of outgoing longwave radiation to space as a response to warming of the Northern Hemisphere associated with the increased poleward oceanic heat transport shown in (b).

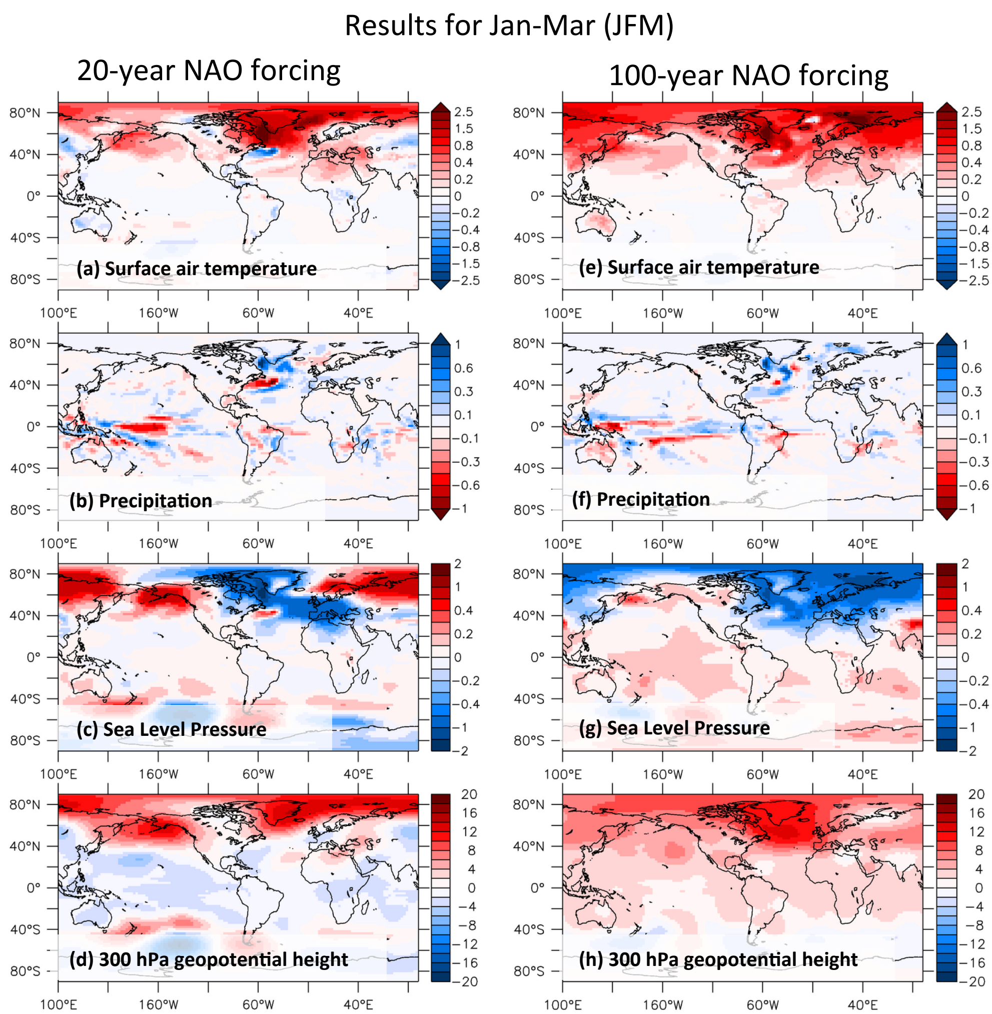

Figure 9 Spatial patterns of simulated response to an increase in the AMOC induced NAO-related surface heat flux anomalies. The responses are averaged over the months of Jan-Mar. Left (right) column shows results from simulations with 20-year (100-year) NAO forcing. Values plotted are regression coefficients of the various fields versus the imposed NAO time series, normalized to represent the response to a two standard deviation change in the NAO-induced fluxes. Left column are results for a 20-year timescale of flux forcing, showing fields 7 years after maximum of imposed NAO flux forcing. The right column shows results for a 100-year timescale of flux forcing, plotted 13 years after maximum of imposed NAO flux forcing.

Results for Jan-Mar (JFM)

20-year NAO forcing

100-year NAO forcing

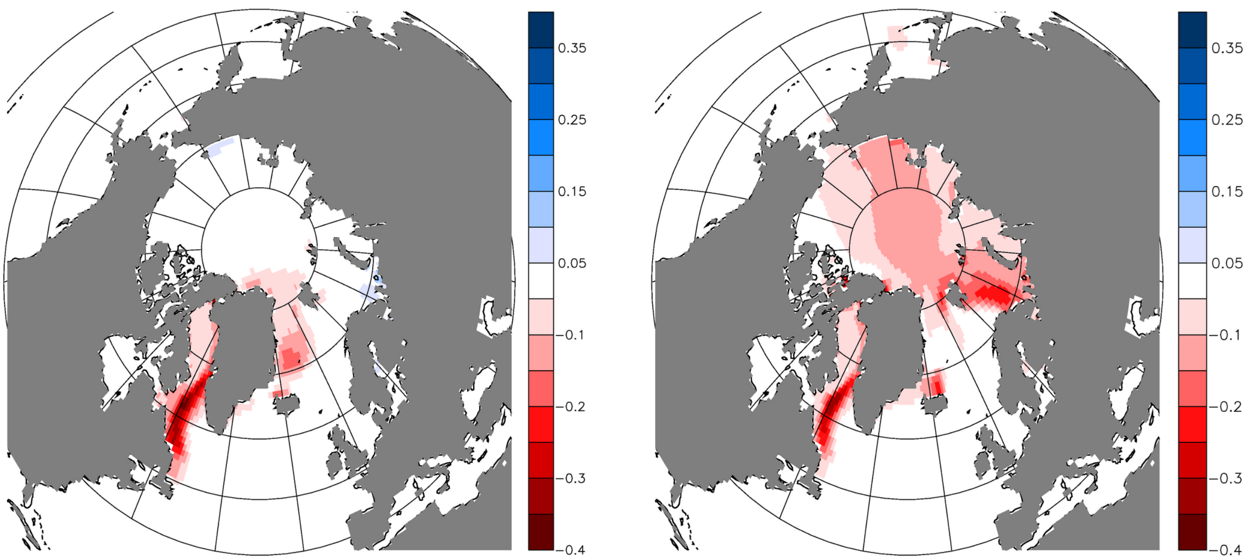

Figure 10 Same as Figure 9, but for sea ice thickness. Units are meters per two standard deviation NAO forcing.

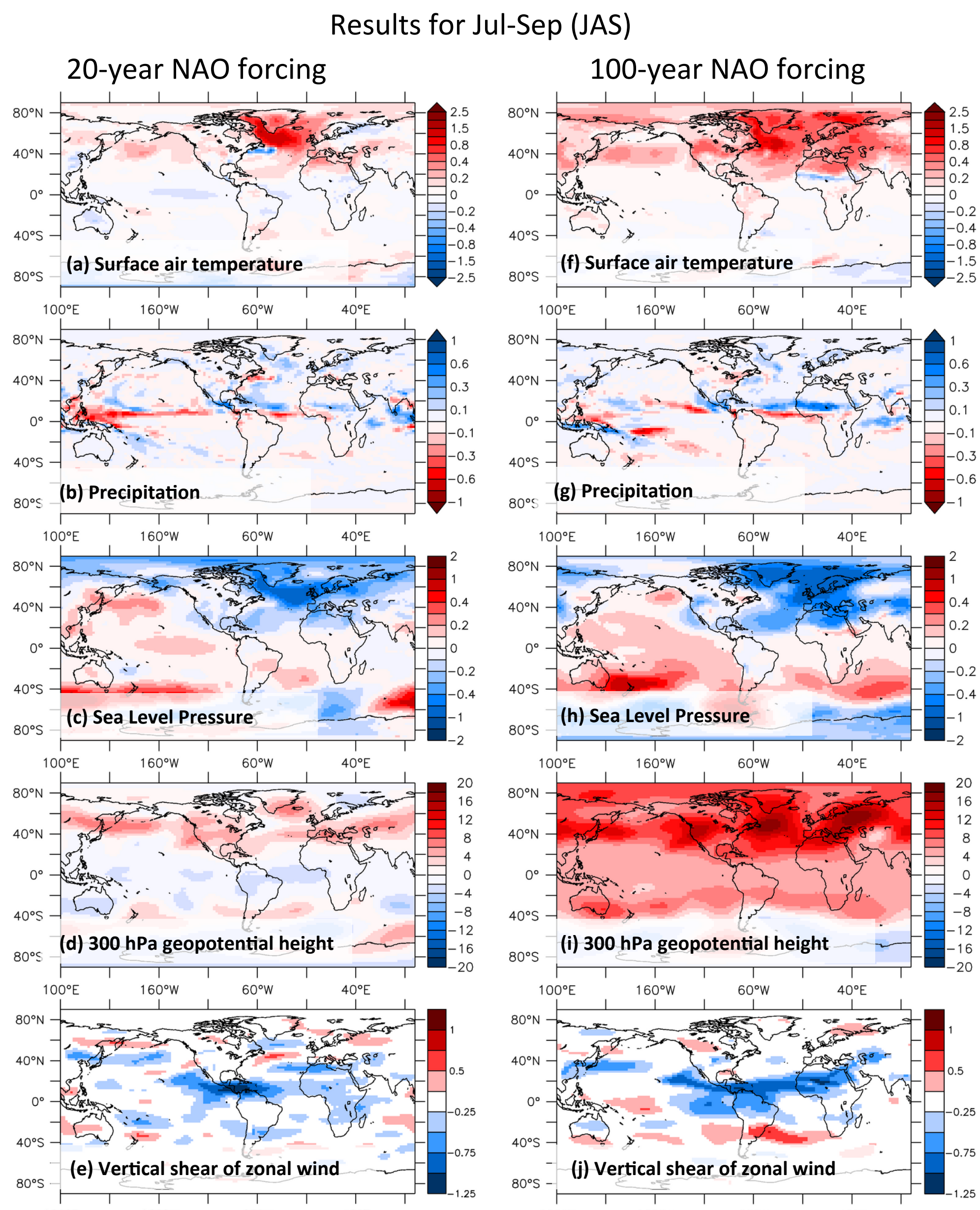

Figure 11 Spatial patterns of simulated response to an increase in the AMOC induced by NAO-related surface heat flux anomalies. The responses are averaged over the months of Jul-Sep. Left (right) column shows results from simulations with 20-year (100-year) NAO forcing. Values plotted are regression coefficients of the various fields versus the time series of the heat flux forcing; these are normalized to represent the response to a two standard deviation change in the NAO-induced fluxes. Left column are results for a 20-year timescale of flux forcing, showing fields 7 years after maximum of imposed NAO flux forcing. The right column shows results for a 100-year timescale of flux forcing, plotted 13 years after maximum of imposed NAO flux forcing. The vertical shear of the zonal wind (bottom row) is calculated as the zonal wind at 250 hPa minus the zonal wind at 850 hPa.

Results for Jul-Sep (JAS)

20-year NAO forcing

100-year NAO forcing

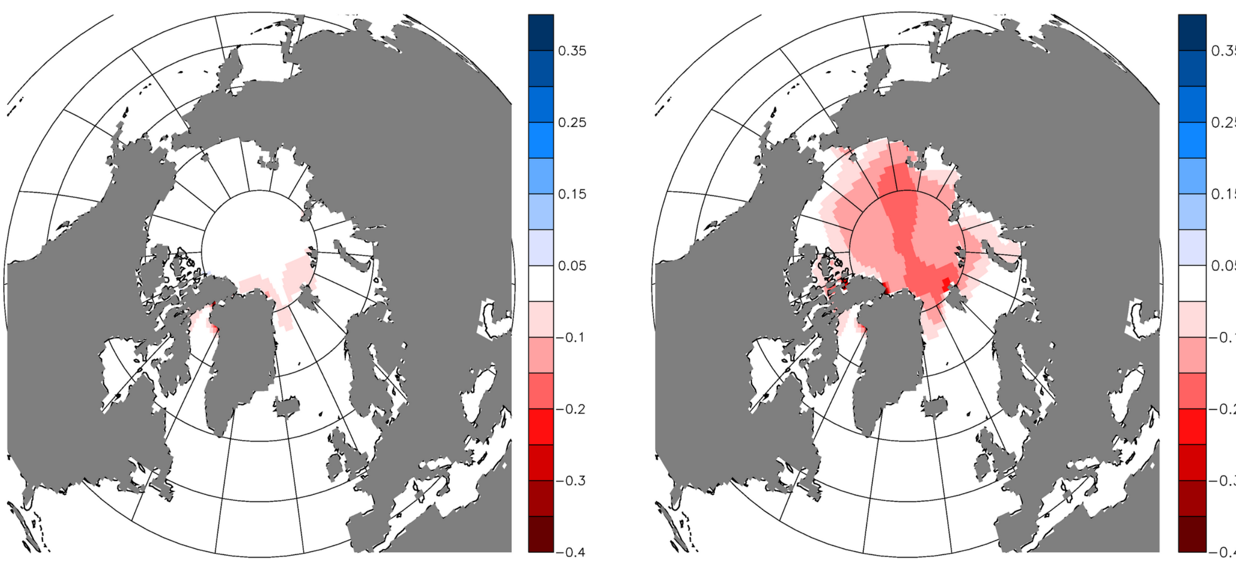

Figure 12 Same as Figure 11, but for sea ice thickness. Units are meters per two standard deviation NAO forcing.

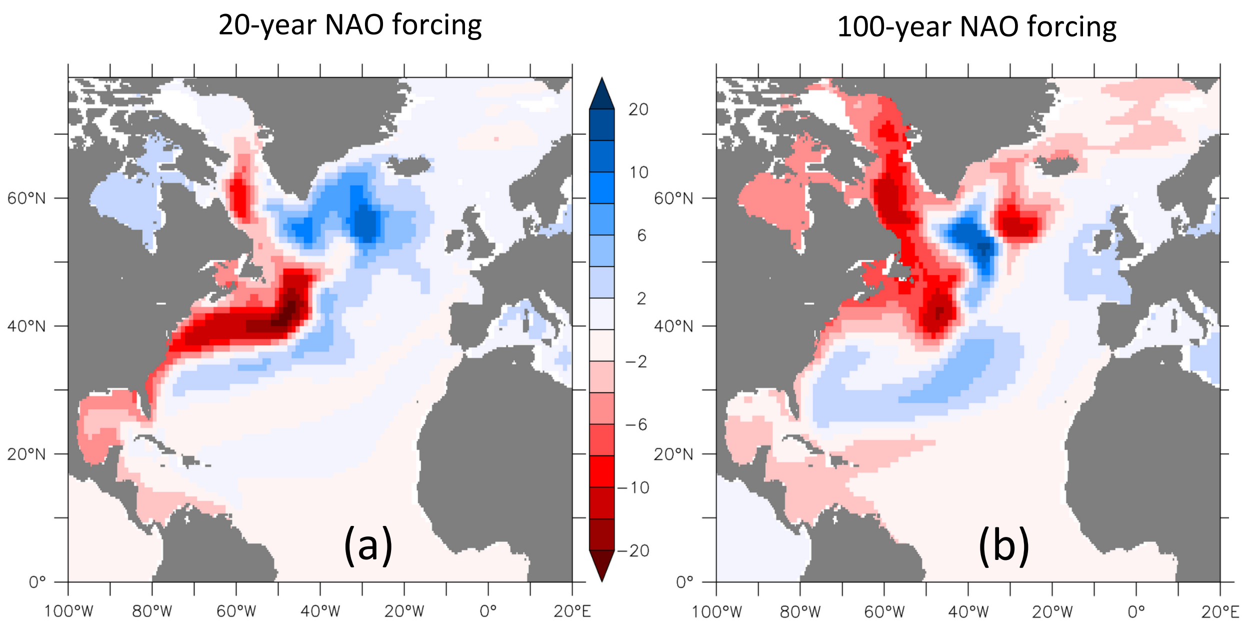

Figure 13 Regression of annual mean sea level height anomaly versus the time series of NAO forcing, expressed as the difference in cm between a positive one standard deviation NAO forcing and a negative one standard deviation NAO forcing. For both cases the maps are representative of conditions 6 years after the maximum NAO flux forcing. (a) Case with NAO-forcing at 20 years. (b) Case with NAO-forcing at 100 years.

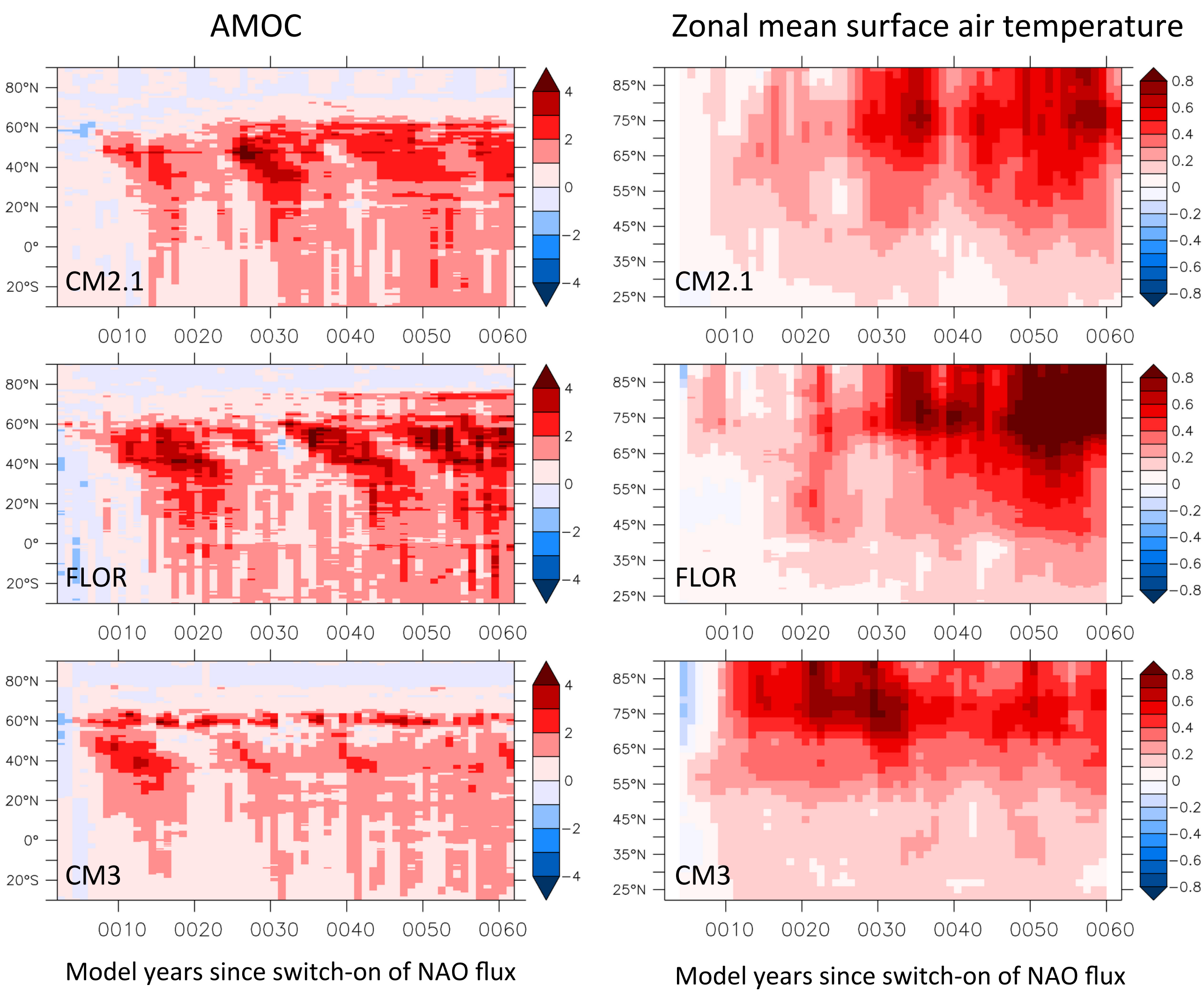

Figure 14 Response of AMOC (left column) and zonally averaged surface air temperature (right column) to sudden switch on of NAO related heat flux forcing. Top row is from CM2.1, middle row from FLOR, and bottom row from CM3. Units are Sv for AMOC changes, and K for temperature changes. Time is listed along the x-axis in years, latitude is on the y-axis.

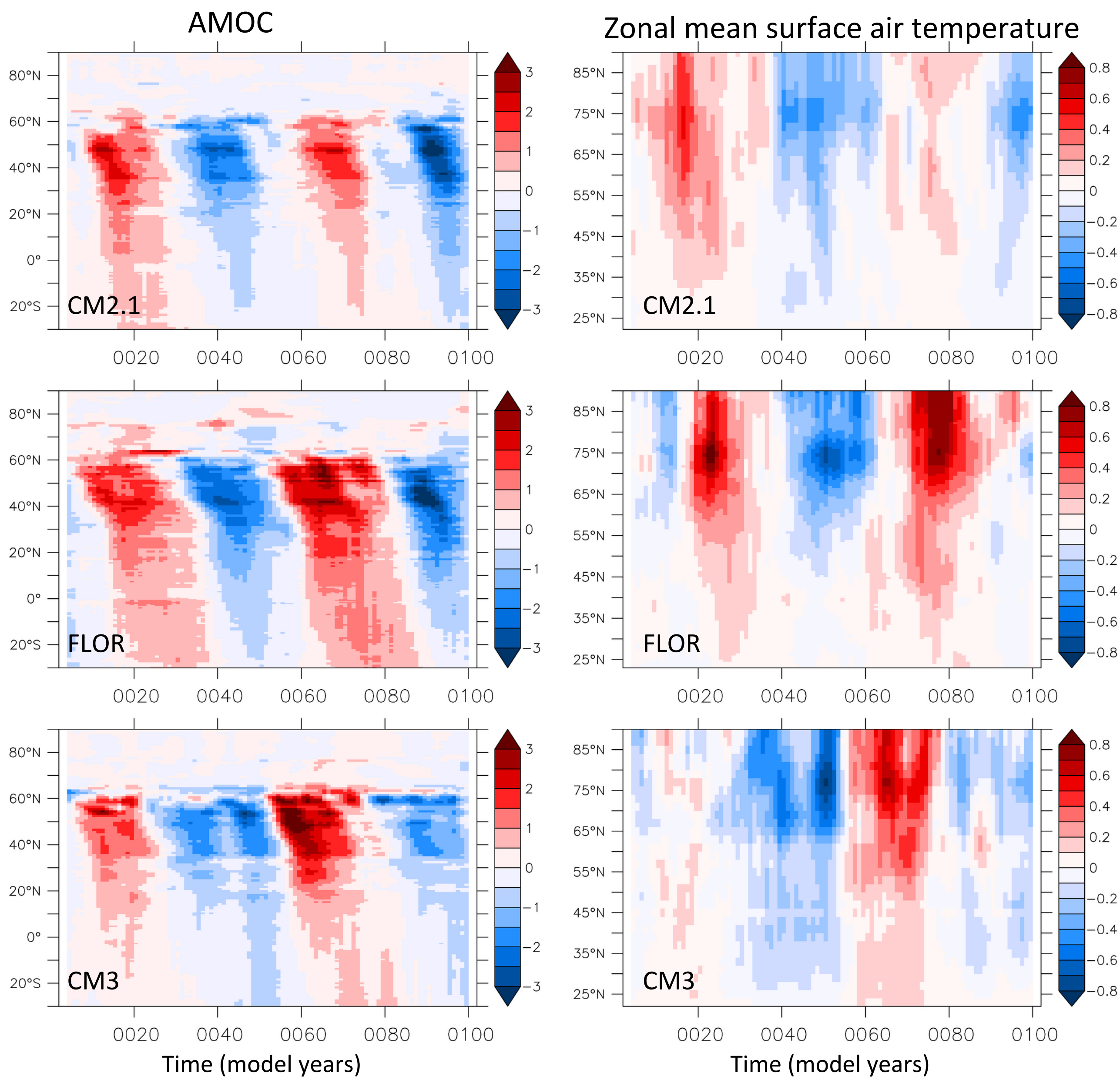

Figure 15 Response of AMOC (left column) and zonally averaged surface air temperature (right column) to sinusoidal NAO heat flux forcing with amplitude of one standard deviation of the NAO time series and period of 50 years. Top row is from CM2.1, middle row from FLOR, and bottom row from CM3. Units are Sv for AMOC changes, and K for temperature changes. Time is listed along the x-axis in years, and latitude along the y-axis.

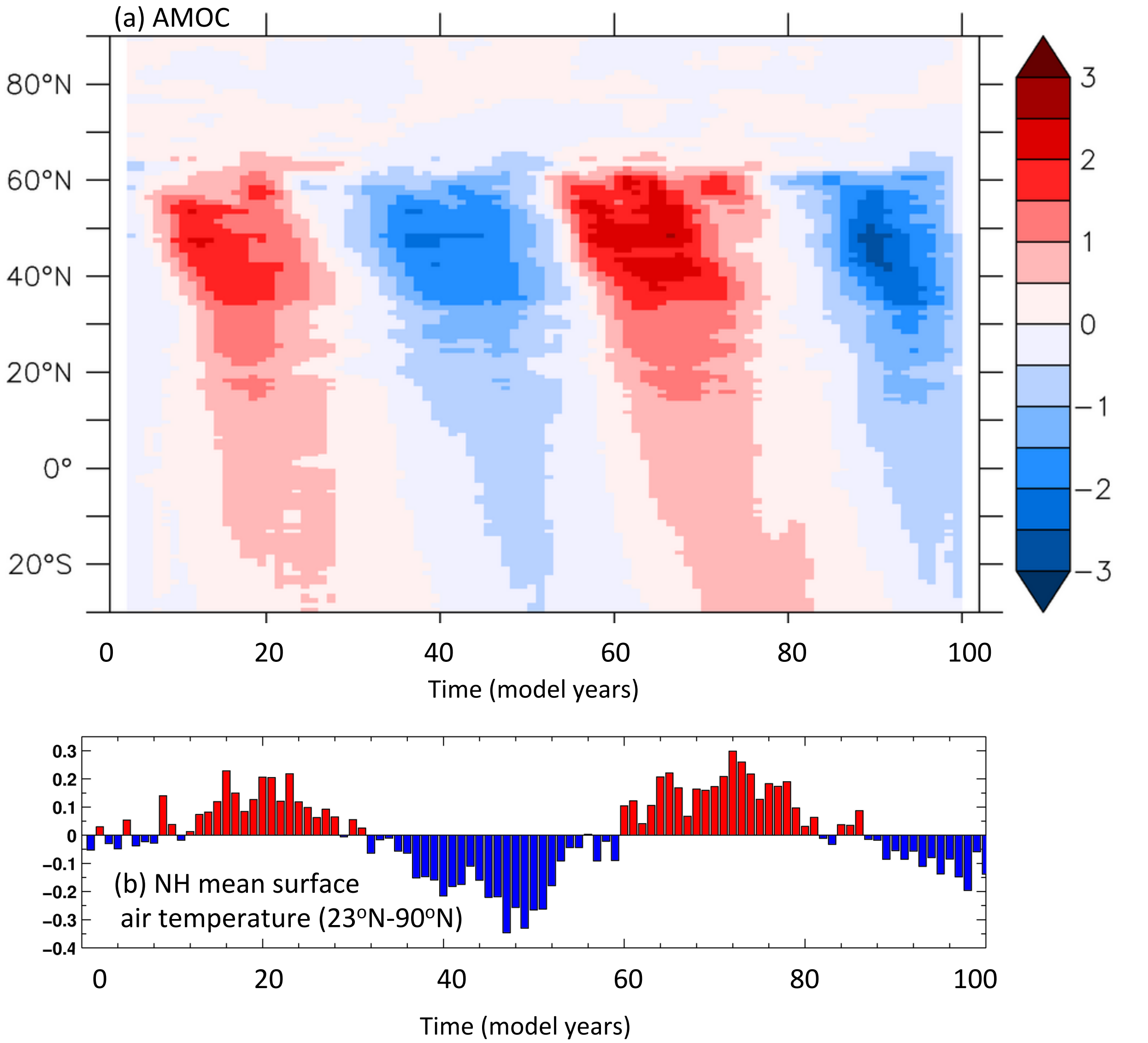

Figure 16 Response to 50-year NAO heat flux forcing calculated as the ensemble mean response from CM2.1, FLOR, and CM3. We first calculate the ensemble mean using each model, and then compute the mean of those three ensemble means. Time is listed in years along the x-axis, indicating years since switching on the NAO-related heat fluxes. (a) AMOC response as a function of latitude and time, units are Sv. (b) NH mean surface air temperature response, averaged over the domain 23°N-90°N. Units are K.